«ФИЗИКА ЭЛЕМЕНТАРНЫХ ЧАСТИЦ И АТОМНОГО ЯДРА»
1997, ТОМ 28, ВЫП.1

УДК 539.12.01

THERMODYNAMICS OF STRONG INTERACTIONS

V.I.Yukalov, E.P.Yukalova

Joint Institute for Nuclear Research, Dubna, 141980 Russia
and Queen's University, Kingston, Canada

The state of art in studying thermodynamic properties of hot and dense nuclear matter is reviewed with the special emphasis on the confinement–deconfinement transition between hadron matter and quark–gluon plasma. The most popular models used for describing deconfinement are analysed, including statistical bootstrap models, pure phase models, the model of clustered quarks, and the string–flip potential model. Predictions of these models are compared with the lattice numerical simulations. It is concluded that precursor fluctuation effects must be taken into account in order to get a realistic description of deconfinement transition. The existence of precursor fluctuations is in line with the dynamical confinement scenario and suggests that deconfinement cannot be considered as a transition between pure hadron and quark–gluon phases. All this supports the concept of cluster coexistence advocated by the authors of this review: Quark–gluon plasma and hadron clusters are different quantum states of the same system, so that any statistical model pretending to treat nuclear matter under extreme conditions must incorporate into itself the probability of these different channels. The ways of constructing statistical models with plasma–cluster coexistence are discussed and thermodynamic properties of such models are analysed.

В обзоре изложены подходы к описанию термодинамических свойств горячей и плотной ядерной материи. Особое внимание уделяется переходу конфайнмент-деконфайнмент, происходящему между адронной материей и кварк-глюонной плазмой. Проанализированы наиболее известные модели описания деконфайнмента, включая модели статистического бутстрапа, модели чистых фаз, модель кластеризованных кварков и струнные потенциальные модели. Предсказания этих моделей сравниваются с решеточными вычислениями. Делается вывод, что для реалистического описания деконфайнмента необходимо учитывать предпереходные флуктуационные эффекты. Существование переходных флуктуаций согласуется со сценарием динамического конфайнмента и показывает, что деконфайнмент нельзя рассматривать как переход между чистыми адронной и кварк-глюонной фазами. Все это поддерживает концепцию сосуществования кластеров, пропагандируемую авторами данного обзора: кварк-глюонная плазма и адронные кластеры — это различные квантовые состояния одной системы, поэтому любая статистическая модель, претендующая на описание ядерной материи в экстремальных условиях, должна включать в себя вероятность этих различных каналов. Обсуждаются способы построения статистических моделей, учитывающих сосуществование плазмы и кластеров, и анализируются термодинамические свойства этих моделей.

1. INTRODUCTION

One of the most intriguing problems of high energy physics is the possibility of transforming the nuclear matter composed of hadrons into the phase consisting of their fundamental constituents, quarks and gluons. This phase, because of the apparent analogy with the electron–ion plasma, is called the quark–gluon plasma.

The transformation of the hadron matter into the quark–gluon plasma is named deconfinement; the inverse process, respectively, being called confinement. The deconfinement transition is somewhat similar to the ionization of atoms. The literature devoted to this phenomenon is so numerous that, not to overload the list of references, we shall cite here mainly review papers, when these are available, and in which the reader can find thousands of references to original works. The specific feature of the present review is that we concentrate on the statistical models of strongly interacting systems under extreme conditions, when non–hadronic degrees of freedom become important and deconfinement occurs.

The possibility that quark degrees of freedom can come into play in the process of relativistic nuclear collisions at already achieved accelerator energies was advances by A.M.Baldin [1] who predicted and explained the commulative effect as a manifestation of the formation in the colliding nuclei of multiquark droplets.

In order that quark–gluon degrees of freedom would be essential, special conditions are necessary, like high temperature or density. From quantum chromodynamics it is known that at asymptotically high temperature quarks and gluons are really deconfined forming the quark–gluon plasma [2-6]. We also know that at zero temperature and at the normal density of nuclear matter there is complete confinement so that only hadrons exist. But where is the intermediate region in which quark–gluon degrees of freedom become relevant? The characteristic parameters for this region can be estimated as follows.

Nuclear matter in the normal state has the baryon density $n_{0B} = 0.167/fm^3$. The corresponding normal quark density is $\rho_0 \equiv 3n_{0B} = 0.5/fm^3$. The characteristic quark interaction energy in the normal state can be presented as $E_0 = \hbar/\tau_0$, with the interaction time $\tau_0 = a_0/c$, where $a_0 = \rho_0^{-1/3}$ is the mean interquark distance in the normal state. Accepting the system of units in which $\hbar = c = 1$, with the conversion constant $\hbar c = 197.327\ MeV/fm$, we have

$$E_0 = \rho_0^{1/3} = 157\ MeV.$$

Note an interesting relation between this interaction energy and the characteristic baryon energy density $\varepsilon_B \equiv m_N n_{0B}$, in which $m_N \equiv \frac{1}{2}(m_p + m_n) = 939\ MeV$ is the average nucleon mass. Since $\varepsilon_B = 157\ MeV/fm^3$, therefore $E_0 = \varepsilon_B\ fm^3$. Thus, the normal nuclear matter should start to decompose being heated up to the temperature equal to the quark interaction energy E_0, that is up to $\Theta_c \approx 160\ MeV$.

If one wishes to destroy the hadron matter by compression, one has to reach a density of about the density of quarks inside a nucleon. This characteristic density is $\rho_c \equiv 3/v_N$, where $v_N \equiv (4\pi/3)r_N^3$ is the nucleon volume. Taking for the nucleon radius $r_N = 0.9\ fm$, we get $v_N = 3\ fm^3$. From here

$$\rho_c = 2\rho_0 = 1/fm^3.$$

This tells us that the hadron matter should start desintegrating being compressed up to the density $\rho_c \approx 2\rho_0$.

As we see, the expected critical temperature and density are fairly low. Such conditions certainly existed in the early Universe about $10^{-5} \div 10^{-4} sec$ after the Big Bang and are likely to exist in the interior of neutron stars [7].

More important is the common belief that such conditions can be created in the process of relativistic heavy ion collisions, even with existing accelerators, thus opening the path for experimental observation of the quark-gluon plasma in the laboratory [8-14]. Analogous relativistic nuclear collisions can also be studied in cosmic ray experiments [8]. The density of matter inside a fireball formed by two collided ions can reach $10\rho_0$.

All models of the formation of the quark–gluon plasma in nuclear collisions require the information about its rate of thermalization. Does the matter inside a fireball thermalize sufficiently fast, so that a thermodynamic description makes sense? For this, the thermalization time must be shorter than the fireball lifetime $\tau_f \sim 10^{-22} sec$. The thermalization time, or the time of local equilibration, τ_{loc} , can be estimated as follows [13-15]. The local equilibrium time writes as $\tau_{loc} = \lambda/c$, in which $\lambda = (\rho\sigma)^{-1}$ is the mean free path of a particle in a medium; $\rho = a^{-3}$, the density of matter; a , average interparticle distance; $\sigma \sim b^2$, cross section; b , interaction radius. Accepting the values $a \sim b \sim 1 fm$ typical of nuclear matter, we have $\lambda \sim 1 fm$ and $\tau_{loc} \sim 10^{-23} sec$. Because of the inequality $\tau_{loc} \ll \tau_f$, the thermalization inside a fireball is likely to be reached.

The possibility of speaking about the thermodynamics of strong interactions, separately from electromagnetic and weak interactions, is based on the fact that it is just this type of interaction which in many cases plays the dominant role. Really, the dimensionless coupling constant of strong interactions $\alpha_s \approx 1$ is much larger than the coupling constants of electromagnetic interactions, $\alpha_e \approx 1/137 \sim 10^{-2}$, and of weak interactions, $\alpha_w \sim 10^{-5}$, to say nothing of the coupling constant of gravitational interactions, $\alpha_g \sim 10^{-12}$. The corresponding interaction times, at the energy $1\ GeV$ characteristic of high–energy physics, are $\tau_s \sim 10^{-24} sec$ for strong interactions, $\tau_e \sim 10^{-21} sec$ for electromagnetic interactions, and $\tau_w \sim 10^{-10} sec$ for weak interactions. Therefore, during the lifetime of a fireball $\tau_f \sim 10^{-22} sec$ electromagnetic and weak interactions do not play any role. In the interval of time $\tau_{loc} < t < \tau_f$ inside a fireball there may exist an equilibrium state of strongly interacting particles.

The sole consistent way of calculating thermodynamic characteristics in the frame of quantum chromodynamics is perturbation theory, which is quite similar to that of quantum electrodynamics [16,17]. However, the effective coupling parameter of strong interactions becomes small only at asymptotically high temperatures. In the most interesting region of temperatures around $\Theta_c \approx 160\ MeV$, where deconfinement occurs, the coupling parameter is large and perturbation the-

ory does not work. For describing the whole range of thermodynamic variables several statistical models have been suggested .

2. STATISTICAL BOOTSTRAP MODELS

The usefulness of applying statistical methods for considering the heated and compressed nuclear matter has been understood long time ago. Let us mention, e.g.,Fermi [18].

The first statistical model of nuclear matter under extreme conditions, such as being realized inside fireballs, has been proposed by Hagedorn [19] (see also [20]) and called the statistical bootstrap model. In this approach it is assumed that, at zero baryon density $n_B = 0$, various hadrons can be generated from vacuum with the mass distribution

$$\rho(m) = \rho_{dis}(m) + \rho_{con}(m); \qquad m \in [0, \infty),$$

in which the first and the second terms correspond to discrete and to continuous mass spectra respectively,

$$\rho_{dis}(m) = \sum_i \zeta_i \delta(m - m_i) \left[1 - \Theta(m - m_0)\right],$$

$$\rho_{con}(m) = \Theta(m - m_0) \frac{a_0}{m^{5/2}} \exp\left(\frac{m}{\Theta_0}\right),$$

where $\Theta(\cdot)$ is the unit–step function; ζ_i , a degeneracy number for spin–isospin states; and the parameters are

$$m_0 = 1000\ MeV, \quad a_0 = 6.5 \times 10^3\ MeV^{3/2}, \quad \Theta_0 = 160\ MeV.$$

The pressure for the ideal hadron gas is written in the classical Boltzmann approximation,

$$p = \Theta \int \rho(m) \exp\left(-\beta\sqrt{k^2 + m^2}\right) \frac{d\vec{k}}{(2\pi)^3} dm,$$

where Θ is temperature in energy units, and β is inverse temperature, $\beta\Theta \equiv 1$.

As can be easily checked, the pressure in this model diverges for all $\Theta \geq \Theta_0$. From here it was concluded [19] that Θ_0 is the limiting temperature of the Universe. The concept of the existence of a maximal temperature of the Universe is, of course, quite artificial, therefore another interpretation of this divergency of pressure has been proposed [20] treating Θ_0 as the deconfinement temperature.

After Collins and Perry [21], the geometrical scenario of the deconfinement became popular [22]. According to this, the increase of temperature or baryon density leads to the rising number of hadrons. The latter are assumed to have finite volumes [23]. When the number of hadrons becomes so high that their close packing occurs, then they fuse into one gigantic hadron occupying the whole system. The Hagedorn temperature Θ_0 is interpreted as the fusion temperature, and the gigantic hadron cluster is identified with the system in the quark–gluon–plasma state. This geometric scenario reminds the percolation transition [24].

Following the geometric interpretation, the bootstrap model was modified [20] invoking the excluded–volume approximation. In this, one considers N particles having the volumes $v_1, v_2, \ldots, v_N$ as moving in the free volume

$$V_N \equiv V - \sum_{j=1}^{N} v_j,$$

where V is the total volume of the system. The pressure in the excluded–volume approximation becomes

$$p = \frac{\Theta}{V} \ln \left\{ \sum_{N=1}^{\infty} \frac{1}{N!} \Theta(V_N) \left[V_N \int \rho(m) \exp\left(-\beta\sqrt{k^2+m^2}\right) \frac{d\vec{k}}{(2\pi)^3} dm \right]^N \right\},$$

where again the Boltzmann approximation is also used. The mass distribution for discrete spectrum is taken in the same form as above, and for continuous spectrum it is slightly modified as

$$\rho_{con}(m) = \Theta(m - m_0) \frac{a_0}{m^\alpha} \exp\left(\frac{m}{\Theta_0}\right),$$

with $\frac{3}{2} < \alpha < \frac{7}{2}$. Now, the pressure is everywhere finite and positive becoming zero at the same temperature $\Theta_d \approx \Theta_0$. The temperature Θ_d, where $p(\Theta_d) = 0$, is interpreted as the temperature of hadron fusion into a gigantic cluster. However, the thermodynamics of the system at $\Theta \to \infty$ has nothing to do with that of the ideal quark–gluon plasma.

To overcome the latter deficiency of the model, it has been argued that taking into account hadron compression can save the situation. This can be done [25] by complicating the mass distribution writing its continuous part as

$$\rho_{con}(m, v) = \Theta(m - b_0 v - m_0)\Theta(v - v_0) a_0 (m - b_0 v)^\alpha \times$$

$$\times v^\gamma \exp\left\{ \frac{4}{3} (\sigma_0 v)^{1/4} (m - b_0 v)^{3/4} \right\},$$

which contains now seven fitting parameters: $m_0, a_0, \alpha, b_0, v_0, \gamma, \sigma_0$.

Now, in accordance with the geometrical scenario, the number of hadrons at low temperature $\Theta < \Theta_d$ is proportional to the free volume, and at high temperatures $\Theta \to \infty$ this number tends to one symbolizing the formation of a gigantic cluster. However, at the 1st order transition temperature Θ_d the number of hadrons $N(\Theta_d, V)$ diverges for any finite volume V, which is unreasonable.

The bootstrap models, in addition to the arbitrariness in postulating the mass distribution, contain internal deficiencies leading to the existence of instabilities contradicting the necessary stability conditions for statistical systems [26,27].

3. PURE PHASE MODELS

An evident idea would be to follow the standard Gibbs prescription for considering phase transitions between two phases. Treating the deconfinement as such a phase transition, one assumes the existence of two types of pure phases. At low temperatures and baryon densities this is a pure hadron phase with features typical of the normal nuclear matter [28], and at high temperature or baryon density this is the quark–gluon phase described by perturbative QCD [17]. Let Ω_1 be the grand potential of the quark–gluon plasma, and Ω_2, that of the hadron matter. According to the Gibbs rule, a phase transition occurs when $\Omega_1(\Theta, \mu_B) = \Omega_2(\Theta, \mu_B)$, where μ_B is the baryon chemical potential. This equality gives a transition line $\Theta_d = \Theta_d(\mu_B)$. Expressing here the baryon potential $\mu_B = \mu_B(n_B)$ through the baryon density, we may write $\Theta_d = \Theta_d(n_B)$.

The possibility of using perturbation theory for the high–temperature quark–gluon plasma is based on the property of asymptotic freedom. According to this property, the running coupling constant

$$\alpha_s(q) \simeq \frac{6\pi}{(11N_c - 2N_f)\ln(q/\Lambda)}\left[1 - \frac{51\ln\ln(q/\Lambda)}{121\ln(q/\Lambda)}\right],$$

in which N_c and N_f are the number of quark colours and flavours, respectively, $\Lambda \approx 200\ MeV$ is a scale parameter, and q is momentum, tends to zero as $q \to \infty$. In the integral over momenta, defining the grand potential, the main contribution, when $\Theta \to \infty$, comes from $q \approx \Theta$. Hence, it is possible to get an expansion in powers of $\alpha_s(\Theta) \equiv g^2(\Theta)/4\pi$ with the effective coupling parameter

$$g^2(\Theta) \simeq \frac{24\pi^2}{(11N_c - 2N_f)\ln(\Theta/\Lambda)}.$$

As a result of this expansion [29], neglecting quark masses, one has for the grand potential

$$\frac{\Omega_1}{V} = -A\Theta^4 + B,$$

in which a nonperturbative term B is included and the notation

$$A \equiv A_0 + A_2 g^2 + A_3 g^3 + A_4 g^4 \ln g$$

is used, where

$$A_0 = \frac{\pi^2}{45}\left[N_c^2 - 1 + \frac{7}{4}N_c N_f + 15 N_c \sum_f \frac{\mu_f^2}{2\pi^2\Theta^2}\left(1 + \frac{\mu_f^2}{2\pi^2\Theta^2}\right)\right],$$

$$A_2 = -\frac{N_c^2 - 1}{144}\left[N_c + \frac{5}{4}N_f + 9\sum_f \frac{\mu_f^2}{2\pi^2\Theta^2}\left(1 + \frac{\mu_f^2}{2\pi^2\Theta^2}\right)\right],$$

$$A_3 = \frac{N_c^2 - 1}{12\pi}\left(\frac{1}{3}N_c + \frac{1}{6}N_f + \frac{1}{3}\sum_f \frac{\mu_f^2}{2\pi^2\Theta^2}\right)^{3/2},$$

$$A_4 = \frac{N_c^2 - 1}{16\pi^2}N_c\left(\frac{1}{3}N_c + \frac{1}{6}N_f + \sum_f \frac{\mu_f^2}{2\pi^2\Theta^2}\right),$$

μ_f being the chemical potential of an f–flavour quark. Note that the term $O(g^6)$ cannot be calculated by perturbation theory because of unrenormalizable infrared divergences.

Take into account that the number of quark colours is $N_c = 3$, and consider for simplicity the case of zero baryon density $n_B = 0$, so that $\mu_f = 0$. Then the pressure of the quark–gluon plasma is

$$p_1 \equiv -\frac{\Omega_1}{V} = A\Theta^4 - B,$$

with the expansion coefficients of A being

$$A_0 = \frac{8\pi^2}{45}\left(1 + \frac{21}{32}N_f\right), \qquad A_2 = -\frac{1}{6}\left(1 + \frac{5}{12}N_f\right),$$

$$A_3 = \frac{2}{3\pi}\left(1 + \frac{1}{6}N_f\right)^{3/2}, \qquad A_4 = \frac{3}{2\pi^2}\left(1 + \frac{1}{6}N_f\right).$$

The low–temperature hadron phase is often modeled [4,7,30] by a gas of massless noninteracting pions, which for the grand potential yields

$$\frac{\Omega_2}{V} = -\frac{\pi^2}{30}\Theta^4.$$

The corresponding pressure is

$$p_2 \equiv -\frac{\Omega_2}{V} = \frac{\pi^2}{30}\Theta^4 .$$

Equating Ω_1 with Ω_2, or p_1 with p_2, one obtains the deconfinement temperature

$$\Theta_d = \gamma B^{1/4}; \qquad \gamma \equiv \left(A - \frac{\pi^2}{30} \right)^{-1/4} .$$

To check the phase transition order, let us find the latent heat at the transition temperature.

Define the energy density

$$\varepsilon = s\Theta - p + \mu_B n_B$$

and the entropy density

$$s = -\frac{\partial}{\partial\Theta}\left(\frac{\Omega}{V} \right) = \frac{\partial p}{\partial\Theta} .$$

The latent heat density is

$$\Delta\varepsilon_d \equiv \varepsilon_1 - \varepsilon_2 = \Theta_d \Delta s_d \qquad (\Theta = \Theta_d),$$

where $\Delta s_d \equiv s_1 - s_2$ is the entropy density jump at $\Theta = \Theta_d$.

For the considered case we have

$$s_1 = (4A + C)\Theta^3, \qquad s_2 = \frac{2\pi^2}{15}\Theta^3,$$

with the notation

$$C \equiv \Theta\frac{\partial A}{\partial\Theta} = -\frac{33 - 2N_f}{24\pi^2} g^4 \left[A_2 + \frac{3}{2} A_3 g + \frac{1}{2} A_4 \left(1 + 4\ln g \right) g^2 \right],$$

where the equation

$$\frac{\partial g^2}{\partial\Theta} = -\frac{33 - 2N_f}{24\pi^2\Theta} g^4$$

is taken into account. The energy densities are

$$\varepsilon_1 = (3A + C)\Theta^4 + B, \qquad \varepsilon_2 = \frac{\pi^2}{10}\Theta^4 .$$

Thus, for the latent heat one gets

$$\Delta\varepsilon_d = 4B\left(1 + \frac{C}{4}\gamma^4 \right).$$

The nonperturbative term B is usually treated as the bag constant, with $B^{1/4}$ ranging in the interval $(150 \div 300)\ MeV$. For estimates, we may accept the value $B^{1/4} = 225\ MeV$ from the middle of this interval.

One often assumes that the quark–gluon plasma is an ideal gas of free quarks and gluons, that is $g = 0$. If this is so, then for $N_f = 2$ we have $\gamma = 0.72$. The deconfinement occurs at $\Theta_d = 162\ MeV$ being a first–order transition with the latent heat $\Delta\varepsilon_d = 4B \approx 1\ GeV/fm^3$. The found deconfinement temperature Θ_d almost coincides with the characteristic energy $E_0 = 157\ MeV$ discussed in Introduction. This picture would seem quite reasonable if it would not be absolutely wrong. Really, the effective coupling $g(\Theta) \to \infty$ for temperatures Θ close to the scale parameter $\Lambda \approx 200\ MeV$. Therefore, the assumption that, in the vicinity of the deconfinement point, the quark–gluon plasma is an ideal gas of quarks and gluons is senseless. This would happen only at temperatures at which $g^2(\Theta) \ll 1$, that is, when

$$\Theta \gg \Lambda \exp\left(\frac{24\pi^2}{33 - 2N_f}\right).$$

The latter inequality becomes valid only at very high temperatures $\Theta \gg 10^6\ MeV$.

In this way, nonperturbative effects around the deconfinement transition are very strong, and it is not correct to try taking account of them by the simple addition to the grand potential of a term B.

Some nonperturbative effects can be included into consideration by resorting to the effective–spectrum approximation [31,32], when one postulates for the spectra of quarks and gluons the form $\varepsilon_i(k) = \sqrt{k^2 + m_i^2} + U_i$, in which k is the modulus of momentum; m_i, a mass; U_i, an effective mean field; and $i = q, g$ enumerates quarks and gluons. This approximation yields the results similar to the ideal gas picture: the deconfinement is a first–order transition occurring at $\Theta \approx 160\ MeV$.

The reason why the effective–spectrum and ideal–gas approximations are close to each other can be understood as follows. The effective–spectrum approximation may be interpreted as a result of a renormalization of perturbative series. As an example, we may use the self–similar renormalization [33-36] differing from other resummation techniques by the possibility of checking its range of applicability at each step. Consider the coefficient A in the grand potential Ω_1 of the quark–gluon plasma as an effective limit of the sequence $\{f_k(g)\}$ with the initial approximation $f_0(g) = A_0 + A_2 g^2$, the first approximation $f_1(g) = f_0(g) + A_3 g^3$, and so on. The simplest variant of the self–similar renormalization [33-36] gives the renormalized coefficient

$$A^* = A_0 + \frac{4A_2^3 g^2}{(A_3 g - 2A_2)^2}.$$

This quantity, as $A_2 < 0$, is finite for all g including $g \to \infty$. In the whole diapason of $g \in [0, \infty)$ the deconfinement temperature does not change much: for $g = 0$, with $N_f = 2$, it is $\Theta_d = 162\ MeV$, while for $g \to \infty$ it is $\Theta_d = 176\ MeV$. However, the renormalized value A^* is truthful only when the self-similar renormalization is stable [37-40]. For this we need that the corresponding mapping multiplier $M_1(g)$ and the Lyapunov exponent $\Lambda_1(g)$ would satisfy the stability conditions: $|M_1(g)| < 1$ and $\Lambda_1(g) < 0$. In the considered case

$$M_1(g) = 1 + \Lambda_1(g), \qquad \Lambda_1(g) = \frac{3A_3}{2A_2} g.$$

The Lyapunov exponent, since $A_2 < 0$ and $A_3 > 0$, is always negative. The condition $|M_1(g)| < 1$ holds only for $g < 4|A_2|/3A_3$, that is for $g \leq 1$.

Thus, the renormalization of the grand potential, starting from the perturbative expression, does not essentially change the results. And it is clear why: Really, the ideal-gas picture, which makes the basis of the perturbative expansion, contains no information on bound states that should appear as the coupling constant g increases. The situation with the quark-gluon plasma is somewhat similar to that of the electron-ion plasma in which there can exist bound as well as free electron states [41].

The value of the deconfinement temperature obtained in pure-phase models can be quite reasonable, in the same way as the simple estimate of Introduction is such. However, it would be hard to believe that these models can correctly describe the character of the deconfinement transition and the behaviour of thermodynamic functions.

4. LATTICE NUMERICAL SIMULATION

The idea of using a discrete space-time lattice to regularize quantum field theories opened the entire repertory of statistical physics for the analysis of nonperturbative properties of these theories. The application of Monte Carlo simulation techniques turned out to be a powerful approach allowing to perform a quantitative study of nonperturbative aspects of quantum chromodynamics. The lattice reformulation of QCD has been described in several surveys (e.g., [4,29,42]), therefore below we only slightly touch the principal points of this approach. We shall mainly discuss the predictions of the lattice QCD and its simplified variants for the deconfinement transition.

The first step towards the finite temperature study of QCD consists of introducing the imaginary time $t = -i\tau$ and of rewriting the partition function as a path integral of the exponential of the Euclidean Lagrangian density over all fields in the problem. The second step defines the cubic four-dimensional lattice

with the sites $x = \{\vec{x}, \tau\}$, where $\vec{x} \in \mathbf{Z}_3$ is a real–space lattice vector and $\tau \in \mathbf{Z}_1$ is conventionally called the temporal variable. The lattice spacings in the spatial and temporal directions are denoted by a_σ and a_τ, respectively. If N_σ and N_τ are the number of sites in the corresponding directions, then the volume V and the temperature Θ of the system are given by $V \equiv (N_\sigma a_\sigma)^3$ and $\beta \equiv N_\tau a_\tau$, where $\beta \equiv \Theta^{-1}$.

A gauge–invariant theory on the lattice is usually formulated in terms of link variables U_x^μ and site variables $\psi(x)$ and $\bar{\psi}(x)$. The link variable U_x^μ is associated with a link leaving site x in a direction $\mu = 1, 2, 3, 4$ and it is a matrix $U_x^\mu \in SU(N_c)$ in the space of colour indices, N_c being the number of colours. The site variables $\psi(x)$ and $\bar{\psi}(x)$ are associated with each site x of the lattice and they carry colour, flavour and spin indices. Also, $\psi(x)$ and $\bar{\psi}(x)$, representing fermion fields, are treated as Grassman variables. The link and the site variables satisfy the periodicity conditions

$$U^\mu_{\vec{x},0} = U^\mu_{\vec{x},\beta}, \qquad \psi(\vec{x}, 0) = -\psi(\vec{x}, \beta).$$

Then, in terms of these variables, the partition function is written in the form of a path integral

$$Z = \int \prod_x \prod_\mu \prod_{x'} \mathrm{e}^{-S} dU_x^\mu d\psi(x') d\bar{\psi}(x'),$$

in which the action

$$S = S(U_x^\mu, \psi(x')\bar{\psi}(x')) = S_G + S_F$$

consists of a gauge action S_G and a fermionic action S_F. The partition function and other thermodynamic functions are calculated by using the Monte Carlo procedure on a finite lattice of $N_\sigma^3 \times N_\tau$ sites, the maximal number of sites in each direction being around $N_\sigma = 24$ and $N_\tau = 24$.

The deconfinement transition has been studied, in the frame of the lattice QCD or its pure gauge variants, by many authors. Here we cite only some review–type papers [43-52]. Note, that, in addition to the confinement transition, another transition related to the spontaneous breaking of chiral symmetry can occur. The mechanisms leading to these transitions are seemingly unrelated and it thus has been speculated that QCD may undergo two separate phase transitions. However, the Monte Carlo data for pure gauge models and for the variants with massless quarks suggest that these two transitions coincide. And if the finite masses of quarks are taken into account then the chiral symmetry, strictly speaking, happens only in the limit $\Theta \to \infty$. In what follows we shall speak solely about the deconfinement transition. One of the main discoveries of

the lattice simulation has been the fact that the deconfinement can be of quite different character for different systems.

$SU(2)$ Pure Gauge Model

The common convention is that the deconfinement for such quarkless models is a *second–order transition* occurring at $\Theta_d \approx 210\ MeV$. The errors in calculating the pressure and energy density, related to the finiteness of the used lattice, are around 5% above and 30% below Θ_d .

$SU(3)$ Pure Gauge Model

The deconfinement has been found to be a *first–order transition* at $\Theta_d \approx 225\ MeV$ with the latent heat $\Delta\varepsilon_d \approx \frac{1}{4}\varepsilon_1(\Theta_d)$. The errors of calculating the pressure, energy density and entropy are about 10% above and 30% below Θ_d .

$SU(3)$ Model with Quarks

In the presence of dynamical fermions the situation is by far more complicated as it is difficult to perform high statistics analysis of full QCD on large lattices that would allow a detailed finite size study as it has now been done in the pure gauge sector. Monte Carlo simulations for full QCD with dynamical quarks have by now been performed only for the case of zero baryon density. The transition has been found to be rather sensitive to the choice of quark masses and the number of flavours. It seems that for $N_f > 4$ the transition is first order for all quark masses. For $N_f \leq 4$ the situation is still to some extent uncertain. Nonetheless, there are strong indications that for physical quark masses and $N_f = 3$ the transition is likely to be a continuous crossover, occurring at $\Theta_d \approx 150\ MeV$. However, one should once again stress the uncertainties in the determination of the order of the transition in Monte Carlo simulations, with quarks, even at zero baryon density.

What has been found in the lattice simulations with certainty [52,53] is that nonperturbative effects are quite strong around the deconfinement transition persisting till about $2\Theta_d$. Also, as is seen, no statistical bootstrap or pure phase model is able to describe the variety of different transition orders discovered in the lattice simulations, since these models always predict a sharp first–order transition.

5. DYNAMICAL CONFINEMENT SCENARIO

Correlation functions and related susceptibilities are one of the key tools used for investigating phase transitions [54]. This concerns as well QCD correlation functions [55]. The latter have been intensively studied in lattice numerical

simulations [56-60]. The results of these studies revealed nontrivial effects in the high temperature phase connected with strong quark–antiquark correlations, which was interpreted [56-60] as the existence of hadronic modes, even at high $\Theta > \Theta_d$. De Tar [56] proposed that the high temperature phase might be dynamically confined, in the sense that the long range fluctuations are colour singlet modes, and that the poles and cuts in the linear response functions of the hadronic phase go over smoothly into those of the high temperature one. This scenario of dynamical confinement presupposes that, actually, there is no transition at all, and that there is only a smooth crossover between hadronic matter and the quark–gluon plasma.

It is conjectured [56] that the characterization of the plasma as a weakly interacting gas of quarks and gluons is valid only for short distances and short time scales of the order $1/\Theta$, but that at the scales larger than $1/g^2\Theta$, where g^2 is the running QCD coupling, the plasma exhibits confining features similar to that of the low–temperature hadronic phase. The confinement scale, for instance, at $\Theta \approx 200\ MeV$, is expected to be of order $1\ fm$ and $10^{-24} sec$.

Hatsuda and Kunihiro [61-64] considered the density–density correlation functions of quarks for the Nambu–Jona-Lasinio model with a QCD –motivated effective Lagrangian. They found precursory collective excitations existing in the high–temperature phase and corresponding to correlated $q\bar{q}$ pairs. This means that meson modes do exist above as well as below transition temperature. Really, all poles and cuts of the correlation functions in the momentum–energy representation are the same at all temperatures. Thus, quarks, antiquarks, and gluons should also exist in the low–temperature as well as in high–temperature phase. Such precursor effects are analogous to pretransitional fluctuations in superconductors [65] or superfluid He^3 [66].

The gradual change of the excitation spectrum from hadronic states to quarks and gluons, and the survival of hadronic modes above the transition temperature, have been confirmed for QCD in the instanton–liquid approach [67] and in the magnetic–current approximation [68]. In the latter case, quarks are assumed to interact at high temperature solely through magnetic current–current interactions, the electric ones being screened.

The following picture [68] may serve as an intuitive illustration of the dynamical confinement [56-60]: The current–current interactions persist above Θ_d and force any quark–antiquark pair (and, maybe, every three–quark state) to correlate into colour singlets. As the quarks are moving in the heat bath, the strings connecting them for colour neutrality are constantly breaking and reforming, which can be interpreted as hadrons going in and out of the heat bath.

If the transition between the hadron matter and the quark–gluon plasma is a gradual crossover, as follows from the dynamical confinement scenario, then why in many lattice simulations this transition is found to be of first order? The answer to this question was suggested by Kogut et al. [69] explaining the first

order of this transition merely as due to the finite size of the lattice. Calculating thermodynamic characteristics, such as energy densities, and correlation functions for several lattices with the sizes $8^3 \times 4$, $12^3 \times 4$, $12^3 \times 6$, and $16^3 \times 4$, it has been found [69] that the quark–gluon plasma transition becomes less abrupt as the lattice size increases and the evidence for a first order transition becomes weaker. Lengthy runs for $N_\sigma = 16$ showed no evidence for metastability, so that Kogut et al. [69] concluded that their results suggest that there is no abrupt transition at all, but only a smooth crossover phenomenon.

To describe the coexistence of gluons and glueballs above Θ_d for a quarkless $SU(2)$ system, De Grand and De Tar [57,58] proposed to write the grand potential as the sum

$$\Omega = \Omega_1 + \Omega_2,$$

$$\Omega_1 = -\Theta V \frac{\zeta_1}{2\pi^2} \int_{k_0}^{\infty} k^2 \ln[1 + n_1(\vec{k})] dk,$$

$$\Omega_2 = -\Theta V \frac{\zeta_2}{2\pi^2} \int_{0}^{k_0} k^2 \ln[1 + n_2(\vec{k})] dk,$$

where Ω_1 corresponds to gluons and Ω_2, to glueballs; ζ_i is a degeneracy factor; the Bose distribution $n_i(\vec{k}) = [\exp\{\beta\varepsilon_i(\vec{k})\} - 1]^{-1}$ contains the spectrum $\varepsilon_i(\vec{k}) = \sqrt{k^2 + m_i^2}$ with the mass $m_1 = 0$ for gluons and the mass $m_2 \approx 1000\, MeV$ for glueballs. The cut–off momentum k_0 is postulated, to fit lattice data, to be $k_0 \to \infty$ below Θ_d and $k_0 = 2.86\Theta_d[\Theta_d/(\Theta - \Theta_d)]^{0.3}$ above Θ_d. This phenomenological model describes only the second–order transition in pure $SU(2)$ systems. The temperature dependence of the cut–off momentum k_0 is too arbitrary to permit a straightforward generalization to systems containing quarks as well as various hadrons.

The main value of the dynamical confinement scenario is the clear understanding that hadron and quark–gluon degrees of freedom, generally, coexist.

6. CLUSTERED QUARK MODEL

A model in which quarks could coexist with three–quark clusters, that is, nucleons has been suggested by Clark et al. [70] for zero temperature and considered by Bi and Shi [71] at finite temperatures. Nucleons and quarks in this model are intermixed inside the same system. This kind of mixture should be distinguished from the Gibbs mixture, in which different phases are separated in space having only a common interphase boundary (see [15]). The quark–nucleon

mixture is rather similar to a binary liquid mixture [72]. A two–component system can, generally, stratify in space if there are no chemical reactions between components. The quark–nucleon mixture does not stratify because of the possibility of formation and decay of nucleon clusters, which is taken into account by the relation $\mu_N = 3\mu_q$ between the nucleon, μ_N, and quark, μ_q, chemical potentials. Since it is assumed that inside a nucleon bag and outside it the QCD vacuum is different, the nonstratified mixture corresponds to nonuniform, or unhomogeneous, vacuum. In some sense it reminds the twinking vacuum discussed with respect to the instanton–liquid picture of the QCD vacuum [29]. A nucleon can be interpreted as a droplet of a denser phase inside the rarified plasma phase. Nucleons among quarks are alike fog drops in air. Another analogy is magnetic bubbles in magnets [73].

Clark et al. [70] used the excluded–volume approximation when particles move not in the whole volume V but only in the free volume $V_0 = V - N_N v_N$, where N_N is the number of nucleons of the volume v_N each, defined by the bag model. This renormalizes the volume $V \to \xi V$ by the factor $\xi \equiv V_0/V = 1 - \rho_N v_N$, where $\rho_N \equiv N_N/V$ is the nucleon density. Then, e.g., the baryon density takes the form

$$n_B = \xi \int \left[\frac{1}{3}\zeta_q \left(1 - \frac{2\alpha_s}{\pi} \right) n_q(\vec{k}) + \zeta_N n_N(\vec{k}) \right] \frac{d\vec{k}}{(2\pi)^3},$$

in which, in addition to the geometrical interaction taken into consideration by the factor ξ, the perturbative quark–quark interaction is simulated by the factor $1 - 2\alpha_s/\pi$. The Fermi distributions $n_i(\vec{k})$ contain the free spectra $\omega_i(\vec{k}) = \sqrt{k^2 + m_i^2} - \mu_i$. The energy density reads

$$\varepsilon = \varepsilon_q + \varepsilon_N + B,$$

$$\varepsilon_q = \xi\zeta_q \left(1 - \frac{2\alpha_s}{\pi} \right) \int \varepsilon_q(\vec{k}) n_q(\vec{k}) \frac{d\vec{k}}{(2\pi)^3},$$

$$\varepsilon_N = \xi\zeta_N \int \varepsilon_N(\vec{k}) n_N(\vec{k}) \frac{d\vec{k}}{(2\pi)^3},$$

where the nonperturbative energy is given by a bag constant B.

Comparing the grand potentials for this model with $B^{1/4} = 171\ MeV$ and those of pure quark and of pure nucleon phases, it was found that the mixed clustered matter is more profitable at $n_B > 8n_{0B}$ and $\Theta \leq 50\ MeV$. Of course, one should not take too seriously the numerical predictions of this model which is too oversimplified to be realistic. For instance, pions and gluons are not considered here although they should play an important role in the deconfinement

transition. Thus, pion fields make a nucleon bag unstable at quite moderate density and temperature [74,75] close to those discussed in Introduction.

The most valuable in the clustered quark model is the idea of nonuniform vacuum containing such local fluctuations that nucleons can be formed floating in the surrounding quark matter.

7. STRING–FLIP POTENTIAL MODEL

An extreme realization of the dynamical confinement scenario is given by the string–flip potential model [76-81] based on the quantum–mechanical Hamiltonian

$$H(\vec{r}_1,\ldots,\vec{r}_N)=\sum_{i=1}^{N}\left(-\frac{\nabla_i^2}{2m}\right)+V(\vec{r}_1,\ldots,\vec{r}_N)$$

of nonrelativistic quarks. In the interaction term

$$V(\vec{r}_1,\ldots,\vec{r}_N)=\min\sum_{<ij>}\Phi(r_{ij})\qquad(r_{ij}\equiv|\,\vec{r}_i-\vec{r}_j\,|)$$

the minimum is taken over all ways to group N quarks into hadrons, so that the summation actually goes only over $<i,j>$ pertaining to the same hadron consisting of $2,3,6,9,12$ or 15 quarks. Using the variational wave function

$$\Psi(\vec{r}_1,\ldots,\vec{r}_N)=\exp\{-\beta V(\vec{r}_1,\ldots,\vec{r}_N)\}D(\vec{r}_1,\ldots,\vec{r}_N),$$

in which β is a variational parameter and $D(\ldots)$ is a free Fermi gas Slater determinant, one minimizes the energy $E(\beta)=(\Psi,H\Psi)/(\Psi,\Psi)$ with respect to β. This gives $\beta=\beta(\rho)$ as a function of density.

Variational Monte Carlo calculations for this model have been accomplished with the harmonic, $\Phi(r)=\frac{1}{2}m\omega^2r^2$, and linear, $\Phi(r)=\sigma r$, confining potentials. The wave function has been symmetrized with respect to all of the quark coordinates, including these pertaining to different hadrons. This takes into consideration the exchange quark energy which is found [82] to be about $100\,MeV$.

The results show that the quarks always coalesce into the lowest energy set of flux tubes, which is characteristic of an adiabatic approximation to the strong coupling limit of QCD. At low densities $\rho<\rho_0$ quarks cluster into isolated hadrons. As the density increases, the value of $\beta(\rho)$ decreases, first slowly, but at $\rho\approx 1.5\rho_0$ exponentially. For $\rho\geq 2\rho_0$ the wave functions of separate hadrons strongly overlap, which may be interpreted as a transition to the quark matter, although formally all quarks are yet confined. The complete

deconfinement occurs at asymptotically high densities, when $\beta(\rho) \to 0$, and the wave function becomes that of a free Fermi gas of quarks.

The quark–quark pair correlation function was calculated [76,79] using Monte Carlo techniques and the longitudinal response function, using molecular dynamics simulations [83]. At low densities these functions have the properties typical of a set of isolated hadrons. For instance, the pair correlation function has a sharp peak displaying strong correlations between quarks. The form of this function is similar to that of liquids [84,85]. As the density increases, the peak in the pair correlation function relaxes smoothly to that of a Fermi gas of quarks, disappearing completely as $\rho \to \infty$.

Thus, the string–flip model demonstrates a smooth transition from hadron matter at low densities to a free Fermi gas of quarks at high densities. Quarks at all densities are to some extent confined becoming an absolutely free gas only in the limit $\rho \to \infty$.

The main difficulty in dealing with this model is the necessity of the minimization of the Hamiltonian interaction term over all strings connecting quarks, which involves complicated Monte Carlo calculations. This procedure is necessary for eliminating colour van der Waals forces between colour singlet hadrons. These forces are present in confining two–body potentials and, if not eliminated, produce large spurious energies in nuclear matter.

However, in a consistent statical approach this kind of divergence can be automatically cancelled if one takes into account the corresponding correlation functions, called smoothing or screening functions, which smooth the interaction potentials in the regions of their divergence [86-88]. It is possible, starting with divergent interaction potentials, to construct regular iterative theory [35,89] for Green functions, whose each step involves only smoothed potentials containing no divergencies. In the lower orders of this correlated iteration theory [35] the situation is such that could be obtained by replacing from the beginning the bare interaction potential by a smoothed one, that is by defining an effective Hamiltonian with a pseudopotential instead of the initial potential [86]. Such a replacement is an approximation neglecting some double and all triple correlations [35].

The Hamiltonian of the string–flip model including the minimization over strings is an effective Hamiltonian, in which this minimization plays the role of smoothing. In lieu of this complicated minimization requiring Monte Carlo techniques, it is equivalent to replace the confining potential by a smoothed one.

Röpke et al. [90-93] have developed a many–body approach to quark–nuclear matter generalizing and simplifying the string–flip model. This approach starts with an effective Hamiltonian

$$H_{eff}(\vec{r}_1, \ldots, \vec{r}_N) = \sum_{i=1}^{N} \left(m_i - \frac{\nabla_i^2}{2m_i} \right) + \frac{1}{2} \sum_{i,j}^{N} V_{eff}(\vec{r}_{ij}),$$

in which m_i stands for the quark masses, and the effective interaction $V_{eff}(\vec{r}) \equiv s(r)\Phi(r)$ is screened by a function $s(r)$ defining the probability that two quarks at distance r are next neighbours. The screening function is to be found from some additional equations. In the case of independent particles with density ρ, one has $s(r) = \exp(-\frac{4\pi}{3}\rho r^3)$. Inside a hadron, when $r \ll a$, where $a \equiv \rho^{-1/3}$ is an average interquark distance in the system, we have $s(r) \simeq 1$, so quarks interact through a bare confining potential. For the quarks pertaining to different hadrons, i.e., when $r \gg a$, we get $s(r) \simeq 0$, which is called the saturation property [91].

The many–body approach to clustering quark matter [90-93] makes it possible to give a unique description of both the clustered hadrons as well as the free–quark phase in the same way as it has been done for the nuclear matter whose nucleons could form the deuteron, triton, and α–particle bound states [94,95]. The total density of clustering matter is a sum $\rho = \sum_i z_i \rho_i$, in which z_i is a compositeness factor and ρ is the density of an i–component of clusters composed of z_i particles each.

In the many–body approach the quark system may contain both quasifree quarks (scattering states) and various clusters (bound states). At zero temperature, nucleons start dissolving at $n_B \approx 4.3 n_{0B}$. At zero baryon density the transition of hadron matter to free–quark phase starts at $\Theta_d \approx 200\ MeV$, where some of meson states are already dissolved. But other bound quark states do exist yet at this temperature. The dissolution of the bound states occurs gradually with temperature. Some mesons survive up to $\Theta \approx 2\Theta_d$. The gradual dissociation of bound states above Θ_d is in agreement with the dynamical deconfinement scenario.

Although the many–body approach provides the principal possibility of treating bound states together with quasifree ones, it has the following technical obstacles. Each bound state is described by a Bethe–Goldstone–type equation for a two– or three–particle Green function, depending on the compositeness of this bound state. This type of equations, as is known, is very difficult to deal with. When there are many bound states interacting with each other as well as with unbound particles, then one has to deal with a system of many interrelated Bethe–Goldstone equations, in addition to several equations for one–particle Green functions. In such a case the problem becomes practically as difficult as chromodynamics itself.

8. CONCEPT OF CLUSTER COEXISTENCE

As follows from the previous Sections, there is need of such a statistical model that could provide a realistic description of clustering matter being at the same time treatable. One almost evident simplification would be, instead

of suffering with a system of Bethe–Goldstone equations, to consider bound clusters as separate objects. This can be understood as a kind of renormalization by integrating out the internal degrees of freedom corresponding to the motion of particles inside each of clusters, so that only the center–of–mass degrees of freedom are left.

Enumerate all possible cluster states, including those of unbound, or free, particles, by the index i. Let $\psi_i(\vec{r}) = [\psi_i^\alpha(\vec{r})]$ be the field operator of an i–cluster; this operator being a column in the space of quantum degrees of freedom indexed by α. The quantum degrees of freedom include spin, isospin, colour and flavour indices. The field operators satisfy the commutation relations.

$$[\psi_i^\alpha(\vec{r}), \psi_j^\gamma(\vec{r}')]_\mp = 0, \qquad [\psi_i^\alpha(\vec{r}), \psi_j^{\dagger\gamma}(\vec{r}')]_\mp = \delta_{ij}\delta_{\alpha\gamma}\delta(\vec{r} - \vec{r}'),$$

where the upper sign stands for Bose and the lower, for Fermi statistics.

Take an effective Hamiltonian in the form

$$H = \hat{E} - \sum_i \mu_i \hat{N}_i, \tag{1}$$

in which the energy operator

$$\hat{E} = \sum_i \hat{E}_i + \sum_{i,j} \hat{E}_{ij} \tag{2}$$

consists of the single–cluster energies

$$\hat{E}_i = \int \psi_i^\dagger(\vec{r}) K_i(\vec{\nabla}) \psi_i(\vec{r}) d\vec{r}, \tag{3}$$

where $K_i(\vec{\nabla})$ is a kinetic–energy operator, and of the interaction energies

$$\hat{E}_{ij} = \frac{1}{2} \int \psi_i^\dagger(\vec{r}) \psi_j^\dagger(\vec{r}') \Phi_{ij}(\vec{r} - \vec{r}') \psi_j(\vec{r}') \psi_i(\vec{r}) d\vec{r}\, d\vec{r}', \tag{4}$$

with the interaction potentials $\Phi_{ij}(\vec{r})$ having the symmetry property

$$\Phi_{ij}(\vec{r}) = \Phi_{ij}(-\vec{r}) = \Phi_{ji}(\vec{r}). \tag{5}$$

In the second term of (1), μ_i is the chemical potential of i-clusters and

$$\hat{N}_i = \int \psi_i^\dagger(\vec{r}) \psi_i(\vec{r}) d\vec{r} \tag{6}$$

is a number–of–cluster operator.

The grand potential

$$\Omega = -\Theta \ln \mathrm{Tr}\, e^{-\beta H} \tag{7}$$

defines the pressure

$$p \equiv -\frac{\Omega}{V} = \frac{\Theta}{V} \ln \mathrm{Tr}\, e^{-\beta H}. \tag{8}$$

The energy density is given by

$$\varepsilon \equiv \frac{1}{V} \langle \hat{E} \rangle, \tag{9}$$

where $\langle \ldots \rangle$ denotes the statistical averaging.

For each kind of clusters we may define their density

$$\rho_i(\vec{r}) = \langle \psi_i^\dagger(\vec{r}) \psi_i(\vec{r}) \rangle, \tag{10}$$

the number of clusters

$$N_i \equiv \langle \hat{N}_i \rangle = \int \rho_i(\vec{r}) d\,\vec{r}, \tag{11}$$

and the average density

$$\rho_i \equiv \frac{N_i}{V} = \frac{1}{V} \int \rho_i(\vec{r}) d\,\vec{r}\,. \tag{12}$$

The number of constituents of an i –cluster is called the compositeness factor z_i. The total number of elementary particles is

$$N = \sum_i z_i N_i, \tag{13}$$

so that the average density of the system can be written as

$$\rho \equiv \frac{N}{V} = \sum_i z_i \rho_i. \tag{14}$$

The chemical potentials μ_i can be defined from the conservation laws accepted for the given system. For example, if the numbers N_i for each sort of clusters are fixed, then (12) gives $\mu_i(\Theta, \rho_i)$. If the total number of constituents (13) is fixed, then from the equilibrium condition $\delta\Omega = 0$ we have

$$\frac{\mu_i}{z_i} = \frac{\mu_j}{z_j}, \tag{15}$$

which, together with (14), defines $\mu_i(\Theta, \rho)$. When neither N_i nor N are fixed, then $\mu_i = 0$.

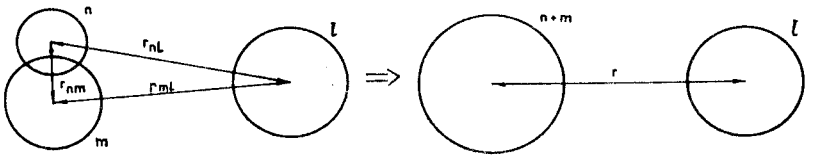

Fig.1. Illustration of a cluster fusion

An important quantity is the *cluster probability*

$$w_i \equiv z_i \frac{\rho_i}{\rho} = z_i \frac{N_i}{N} \tag{16}$$

enjoying the conditions

$$0 \leq w_i \leq 1, \qquad \sum_i w_i = 1, \tag{17}$$

following from (14). With (12), we may rewrite (16) as

$$w_i = \frac{z_i}{N} \int \rho_i(\vec{r}) d\vec{r} \; . \tag{18}$$

If the system of particles can form a number of bound states, then how could we define numerous interactions between clusters? The number of such interactions can be drastically reduced for those clusters whose interaction potentials $\Phi_{ij}(\vec{r})$ have the same type of behaviour at large distance, for example, diminishing as r increases. Consider such clusters with a similar behaviour of $\Phi_{ij}(\vec{r})$. Let two clusters, m and n, coalesce into one, i, so that the compositeness numbers involved in the reaction $m + n \to i$ satisfy the obvious relation $z_m + z_n = z_i$. And let aside be another cluster–spectator, j, as is shown in Fig.1. Assume that the coalescence of the cluster–actors does not influence the cluster–spectator, in the sense that its interaction with the initial two clusters is the same as with that one formed after the coalescence:

$$\Phi_{mj}(\vec{r}) + \Phi_{nj}(\vec{r}) = \Phi_{ij}(\vec{r}). \tag{19}$$

From this assumption, using the conservation law $z_m + z_n = z_i$, we find the relation

$$\frac{\Phi_{ij}(\vec{r})}{z_i z_j} = \frac{\Phi_{mn}(\vec{r})}{z_m z_n}, \tag{20}$$

permitting to express the interaction potentials of different clusters through one calibration potential.

9. SCREENING OF INTERACTION POTENTIALS

The interaction potential $\Phi_{ij}(\vec{r})$ may be divergent for some regions of $\vec{r}$. However, it would not be correct to replace this potential by a smoothed, or screened, one just in the Hamiltonian (1). Such a screening appears in the process of decoupling of binary propagators with taking account of interparticle correlations, as is done in the correlated iteration theory [35]. If one wishes to write an effective Hamiltonian corresponding to a given correlated approximation, it is not sufficient to merely rearrange the operator terms of the Hamiltonian, but a nonoperator correcting term must be added.

Let us illustrate this for the correlated mean-field approximation [35] when the Hamiltonian (1) may be presented in the form

$$H = \sum_i H_i + CV,$$

$$H_i = \int \psi_i^\dagger(\vec{r}) \left[K(\vec{\nabla}) + U_i(\vec{r}) - \mu_i \right] \psi_i(\vec{r}) d\vec{r}, \tag{21}$$

in which the correlated mean field

$$U_i(\vec{r}) = \sum_j \int \bar{\Phi}_{ij}(\vec{r} - \vec{r}') \rho_j(\vec{r}') d\vec{r}' \tag{22}$$

contains the screened potential

$$\bar{\Phi}_{ij}(\vec{r}) = s_{ij}(\vec{r}) \Phi_{ij}(\vec{r}) \tag{23}$$

smoothed by the smoothing function having the symmetry property

$$s_{ij}(\vec{r}) = s_{ji}(\vec{r}) = s_{ij}(-\vec{r}). \tag{24}$$

The nonoperator correcting term in (21) is CV, and this cannot be put zero, as will be shown below.

Since the exact Hamiltonian (1) does not depend on cluster densities, varying the grand potential (7) with respect to $\rho_i(\vec{r})$ we have

$$\frac{\delta \Omega}{\delta \rho_i(\vec{r})} = \left\langle \frac{\delta H}{\delta \rho_i(\vec{r})} \right\rangle = 0. \tag{25}$$

In order that the exact Hamiltonian (1) would be correctly represented by the approximate Hamiltonian (21) requires that the latter must satisfy (25), which yields

$$\frac{\delta C}{\delta \rho_i(\vec{r})} + \frac{1}{V} \sum_j \left\langle \frac{\delta H_j}{\delta \rho_i(\vec{r})} \right\rangle = 0. \tag{26}$$

Substituting here

$$\left\langle \frac{\delta H_i}{\delta \rho_i(\vec{r})} \right\rangle = \int \frac{\delta U_j(\vec{r}')}{\delta \rho_i(\vec{r})} \rho_i(\vec{r}') d\vec{r}',$$

transforms (26) into

$$\frac{\delta C}{\delta \rho_i(\vec{r})} + \frac{1}{V} \sum_j \int \frac{\delta U_j(\vec{r}')}{\delta \rho_i(\vec{r})} \rho_j(\vec{r}') d\vec{r}' = 0. \tag{27}$$

If the smoothing function $s_{ij}(\vec{r})$ does not depend on $\rho_i(\vec{r})$, then (22) gives

$$\frac{\delta U_i(\vec{r})}{\delta \rho_j(\vec{r}')} = \bar{\Phi}_{ij}(\vec{r} - \vec{r}'),$$

and Eq.(27) becomes

$$\frac{\delta C}{\delta \rho_i(\vec{r})} + \frac{1}{V} \sum_j \int \bar{\Phi}_{ij}(\vec{r} - \vec{r}') \rho_j(\vec{r}') d\vec{r}' = 0.$$

The solution of the latter variational equation, up to a constant that can be omitted, is

$$C = -\frac{1}{2V} \sum_{i,j} \int \bar{\Phi}_{ij}(\vec{r} - \vec{r}') \rho_i(\vec{r}) \rho_j(\vec{r}') d\vec{r}\, d\vec{r}'.$$

Note that the Hamiltonian (21) with the obtained correcting term could be derived from (1) with the substitution

$$\psi_i^\dagger(\vec{r}) \psi_j^\dagger(\vec{r}') \psi_j(\vec{r}') \psi_i(\vec{r}) \to$$

$$\to s_{ij}(\vec{r} - \vec{r}') \left\{ \psi_i^\dagger(\vec{r}) \psi_i(\vec{r}) \rho_j(\vec{r}') + \rho_i(\vec{r}) \psi_j^\dagger(\vec{r}') \psi_j(\vec{r}') - \rho_i(\vec{r}) \rho_j(\vec{r}') \right\},$$

corresponding to the correlated Hartree approximation [35].

In general, the smoothing function $s_{ij}(\vec{r})$ is dependent on $\rho_i(\vec{r})$. Therefore, the correcting term is to be found from Eq.(26) or (27). In any case, the correcting term depends on thermodynamic variables through the densities $\rho_i(\vec{r})$. Thus, neglecting this term would disfigure the correct statistical description, and the behaviour of thermodynamic functions could be completely spoiled.

Let us pass to a uniform system when $\rho_i(\vec{r}) = \rho_i$. In principle, a multicomponent system can display a variety of nonuniform states related to the solidification of one or several components. For example, an ensemble of fully

ionized nuclei can form a crystalline lattice immersed in a uniform electron background, which models the high–density matter of white dwarfs [96]. It may be that some heavy cluster components crystallize while others are liquid–like as it happens in superionic conductors [97]. It also may be that heavy clusters form an amorphous solid while light ones move in a conduction band as in glassy metals [98]. In the cores of neutron stars a Gibbs mixture can exist when in some volumes of space a lattice structure appears while others are filled by a liquid–like nuclear matter [99]. We leave aside all these possibilities considering in what follows only uniform systems.

In the uniform case, the mean field (22) becomes

$$U_i(\vec{r}) = \sum_j \Phi_{ij}\rho_i \equiv U_i \tag{28}$$

with the interaction integral

$$\Phi_{ij} \equiv \int \bar{\Phi}_{ij}(\vec{r})d\vec{r}\ . \tag{29}$$

Instead of (25), we have

$$\left\langle \frac{\delta H}{\delta \rho_i} \right\rangle = 0. \tag{30}$$

The correcting equation (27), defining the correcting term, changes to

$$\frac{\delta C}{\delta \rho_i} + \sum_j \frac{\delta U_j}{\delta \rho_i}\rho_j = 0. \tag{31}$$

The field operators, for a uniform system, can be expanded in plane waves,

$$\psi_i(\vec{r}) = \frac{1}{\sqrt{V}} \sum_k a_i(\vec{k})e^{i\vec{k}\vec{r}}; \qquad a_i(\vec{k}) = \left[a_i^{\alpha}(\vec{k})\right].$$

Then an i –cluster Hamiltonian in (21) transforms to

$$H_i = \sum_k \omega_i(\vec{k})a_i^{\dagger}(\vec{k})a_i(\vec{k}), \tag{32}$$

with the effective spectrum

$$\omega_i(\vec{k}) \equiv \varepsilon_i(\vec{k}) - \mu_i, \qquad \varepsilon_i(\vec{k}) \equiv K_i(\vec{k}) + U_i. \tag{33}$$

The number of clusters (11) reads

$$N_i = \sum_k \langle a_i^{\dagger}(\vec{k})a_i(\vec{k})\rangle = \zeta_i \sum_k n_i(\vec{k}), \tag{34}$$

where ζ_i is a degeneracy factor, i.e., the number of quantum states, and

$$n_i(\vec{k}) = \left\{\exp\left[\beta\omega_i(\vec{k})\right] \mp 1\right\}^{-1} \tag{35}$$

is the Bose (upper sign) or Fermi (lower sign) momentum distribution. The cluster density (12) is

$$\rho_i = \zeta_i \int n_i(\vec{k}) \frac{d\vec{k}}{(2\pi)^3}. \tag{36}$$

For the grand potential (7) one gets

$$\Omega = \sum_i \Omega_i + CV,$$

$$\Omega_i = \mp\Theta V \zeta_i \int \ln\left[1 \pm n_i(\vec{k})\right] \frac{d\vec{k}}{(2\pi)^3}. \tag{37}$$

The pressure (8) writes

$$p = \sum_i p_i - C,$$

$$p_i = \pm\Theta\zeta_i \int \ln\left[1 \pm n_i(\vec{k})\right] \frac{d\vec{k}}{(2\pi)^3}. \tag{38}$$

The energy density (9) is

$$\varepsilon = \sum_i \varepsilon_i + C,$$

$$\varepsilon_i = \zeta \int \varepsilon_i(\vec{k}) n_i(\vec{k}) \frac{d\vec{k}}{(2\pi)^3}. \tag{39}$$

The cluster probability (18) becomes

$$w_i = \frac{z_i}{\rho}\zeta_i \int n_i(\vec{k}) \frac{d\vec{k}}{(2\pi)^3}. \tag{40}$$

An additional simplification comes for isotropic systems, which is usually assumed, when $\varepsilon_i(\vec{k}) = \varepsilon_i(k)$, where $k \equiv |\vec{k}|$. Then $\omega_i(\vec{k}) = \omega_i(k)$ and $n_i(\vec{k}) = n_i(k)$. If the spectrum $\omega_i(k)$ is such that the asymptotic properties

$$k^3 \ln \omega_i(k) \to 0 \qquad (k \to 0),$$

$$\omega_i(k) \to \infty \qquad (k \to \infty)$$

hold true, then the cluster pressure and the cluster energy density reduce to

$$p_i = \frac{\zeta_i}{6\pi^2}\int_0^\infty k^3\varepsilon_i'(k)n_i(k)dk,$$

$$\varepsilon_i = \frac{\zeta_i}{2\pi^2}\int_0^\infty k^2\varepsilon_i(k)n_i(k)dk,$$

where $\varepsilon_i'(k) \equiv d\varepsilon_i(k)/dk$.

These are the basic formulas which we shall use in what follows.

10. COEXISTING MULTIQUARK CLUSTERS

The concept of cluster coexistence has been applied first to nuclear matter consisting of different multiquark clusters. The interest to this problem was motivated by the A.M.Baldin cumulative effect [1] and the related discussion of the possible existence of multiquark clusters in nuclei [100,101].

Since at high density or temperature relativistic effects play an important role, the kinetic term of the cluster spectra is taken in the relativistic form $K_i(\vec{k}) = \sqrt{k^2 + m_i^2}$, where m_i is the cluster mass. A system of 3-, 6-, 9-, and 12-quark clusters has been considered in the excluded–volume approximation [102-106]. The 3- and 9-quarks are Fermions, and the 6- and 12-quarks are Bosons. The Bosons with the lowest mass, that is the 6-quarks, can drop down in the Bose–Einstein condensate, when $\omega_6(0) = 0$, which fixes μ_6 . The chemical potentials always satisfy (15).

In the excluded–volume approximation the interaction between clusters is considered geometrically by putting Φ_{ij} zero, but replacing the total volume V by the free volume V_0 ,

$$V \to V_0 \equiv V - \sum_i N_i v_i, \tag{41}$$

where v_i are cluster volumes. This reduces the volume

$$V \to \xi V; \qquad \xi \equiv \frac{V_0}{V} = 1 - \sum_i \rho_i v_i, \tag{42}$$

by a factor $\xi \in [0,1]$. Equivalently, this can be interpreted as a reduction of the degeneracy factor

$$\zeta_i \to \tilde{\zeta}_i \equiv \xi\zeta_i. \tag{43}$$

The reduction factor in (42) and (43) can also be written as

$$\xi = \left(1 + \sum_i \rho_i^{(0)} v_i\right)^{-1}; \qquad \rho_i^{(0)} \equiv \zeta_i \int n_i(k)\frac{d\vec{k}}{(2\pi)^3}.$$

Thus, for the density of clusters, pressure, and energy density one has

$$\rho_i = \tilde{\zeta}_i \int n_i(k) \frac{d\vec{k}}{(2\pi)^3},$$

$$p = \pm\Theta \sum_i \tilde{\zeta}_i \int \ln\left[1 \pm n_i(k)\right] \frac{d\vec{k}}{(2\pi)^3},$$

$$\varepsilon = \sum_i \tilde{\zeta}_i \int \varepsilon_i(k) n_i(k) \frac{d\vec{k}}{(2\pi)^3}. \tag{44}$$

The volumes of clusters are supposed to be related by the equation

$$\frac{v_i}{m_i} = \frac{v_j}{m_j}. \tag{45}$$

This permits to express all cluster volumes $v_i = m_i v_3/m_3$ through the 3-quark volume $v_3 = 4\pi r_3^3/3$ with the radius $r_3 = 0.4\ fm$ of the nucleon core.

The used multiquark parameters are given in Table 1. The 3-quark is a nucleon. The 6-quark mass $m_6 = 1944\ MeV$ corresponds to an average value over the masses of several light narrow dibaryons that are claimed to be observed in experiments [107]. The mass $m_6 = 2163\ MeV$ is taken from the bag-model calculation of Jaffe [108] and the 9- and 12-quark parameters are elicited from the bag model of Matveev and Sorba [109].

The 6-quark probability depends on the value of the mass m_6 as is illustrated in Fig.2. The results for other cluster probabilities are displayed in Figs.3 and 4, where $m_6 = 2163\ MeV$. The probabilities of heavy clusters are always very small: $w_9 < 0.1$, $w_{12} < 0.01$.

As far as we limited here by the length of this review, we shall not discuss in detail the results of our calculations, which can be found in the cited papers. We think that the presented figures speak for themselves: it is better to see once than to listen hundred times.

The coexistence of nucleons with 6-quark clusters has been considered as well in the mean-field approximation [110] with the effective interaction potential

$$\Phi_{ij}(\vec{r}) = 2\pi \frac{a_{ij}}{m_{ij}} \delta(\vec{r}) - \frac{\alpha_\pi}{r} \exp\left(-m_\pi r\right).$$

The first term here is the Fermi pseudopotential for the core interaction with the scattering length $a_{ij} \equiv \frac{1}{2}(a_i + a_j)$, where $a_i \equiv a_{ii}$, and the reduced mass $m_{ij} \equiv m_i m_j/(m_i + m_j)$. The second term is caused by the one-pion exchange; $\alpha_\pi = 0.08$ being the pion coupling parameter and $m_\pi = 140\ MeV$, the pion mass. Again, to reduce the number of model parameters, the relation

Table 1. Multiquark parameters

Mass m_i (MeV)	Compositeness number z_i	Degeneracy factor ζ_i
939	3	4
1944	6	9
2163	6	3
3521	9	4
4932	12	1

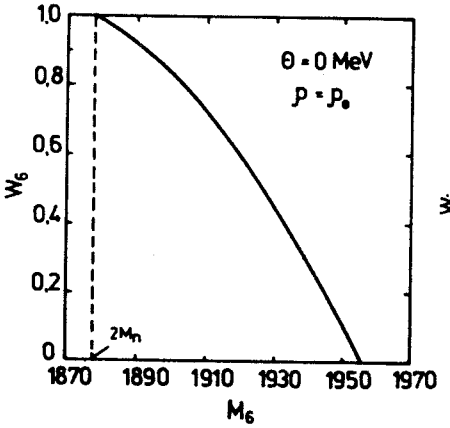

Fig.2. $6q$-probability vs. the mass of a $6q$-cluster at $\Theta = 0$ and $\rho = \rho_0$

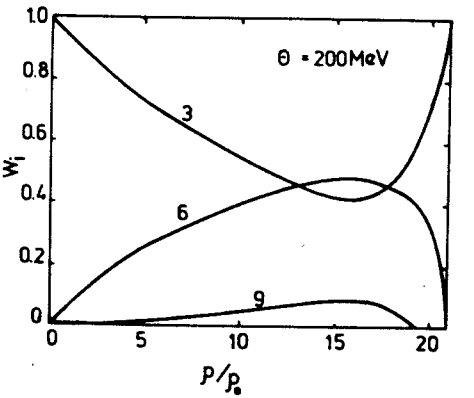

Fig.3. Cluster probabilities as functions of the relative density at $\Theta = 200$ *MeV*

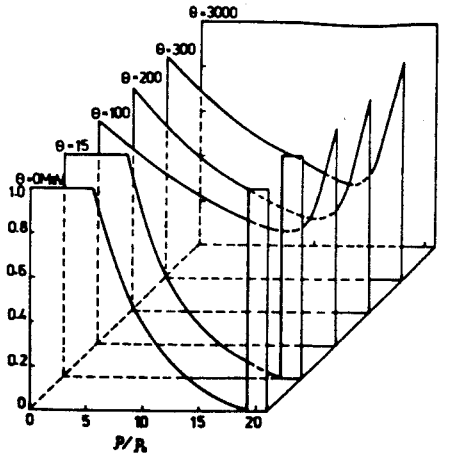

Fig.4. Nucleon probability as a function of the realtive density at different temperatures

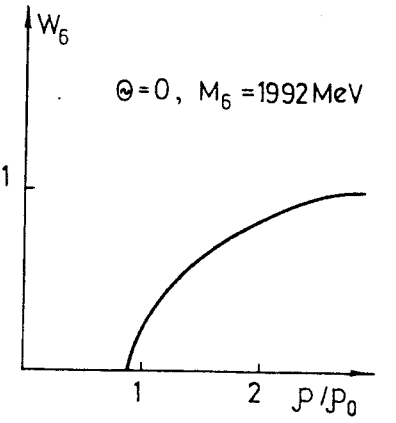

Fig.5. $6q$-probability vs. relative density at $\Theta = 0$

$a_i^3/m_i = a_j^3/m_j$, similar to (45), is accepted. Then, all scattering lengths $a_i = a_3(m_i/m_3)^{1/3}$ are expressed through the nucleon scattering length $a_3 = 1.6fm$. The $6q$-probability is shown in Fig.5.

Note that the mean–field approximation is valid if $|U_i| \ll m_i$, which is true for the densities up to about $10\rho_0$.

The models of this Section serve rather as a qualitative illustration of cluster coexistence. They can have sense only at temperatures and densities much lower than those characteristic of deconfinement, as unbound quarks are not included here.

11. BARYON RICH MATTER

Include into consideration unbound (quasifree) quarks that can, in principle, coexist with multiquark clusters. Whether and when quasifree quarks really coexist should be determined in a self–consistent way from the conditions of thermodynamic advantageousness and stability. To compare the results with those of the previous section, consider again the case of baryon rich matter, when $\rho = 3n_B$, that is when the generation of particles from vacuum can be neglected.

Denote the chemical potential of a quark by $\mu \equiv \mu_q$. Then relation (15) yields $\mu_i = z_i\mu$.

The strengths of characteristic interactions between baryons and between quarks are of the order of or higher than the expected deconfinement temperature, so these interactions must be taken into account. The mean field acting on quarks may be written in a bag–model–motivated form [32] as $U_q = BV/N = B/\rho$. This gives for quarks the spectrum

$$\varepsilon_q(k) = \sqrt{k^2 + m_q^2} + \frac{B}{\rho}. \tag{46}$$

The mean–field term in (46) contains the total quark density ρ , which means that each quasifree quark interacts in the same way with other unbound quarks as well as with quarks entering into bound clusters. The interaction potentials between different baryons can be expressed, basing on relation (20), through the nucleon–nucleon interaction potential $\Phi_{33}(\vec{r})$,

$$\Phi_{ij}(\vec{r}) = \frac{z_i z_j}{9}\Phi_{33}(\vec{r}). \tag{47}$$

There are several such effective potentials obtained from nucleon–nucleon scattering experiments [111] or from analysing the deuteron properties [112]. We opt for the Bonn potential [113]. The common consensus is that thermodynamics of nuclear matter does not depend on the mutual orientation of spins of interacting nucleons. Averaging over spin directions nullifies the spin terms of the interaction

potential. The so–called cut–off terms of the Bonn potential can be neglected, since they start playing an essential role only for very short distances $\leq 0.1 fm$, which would correspond to the baryon density $n_B \geq 10^3 n_{0B}$. We assume that the interaction between any pair of nucleons is the same, because of which in the isospin term of the Bonn potential we put the total isospin $I_1 + I_2 = 1$ describing the interaction between protons or neutrons. The so-obtained radial part of the Bonn potential [113] reads

$$\Phi_{33}(\vec{r}) = \sum_{i=1}^{4} \frac{\alpha_i}{r} \exp(-\gamma_i r) \tag{48}$$

with the parameters

$$\alpha_1 = 16.7, \quad \alpha_2 = 2.7, \quad \alpha_3 = -7.8, \quad \alpha_4 = -2.7,$$

$$\gamma_1 = 738\ MeV, \quad \gamma_2 = 769\ MeV, \quad \gamma_3 = 550\ MeV, \quad \gamma_4 = 983\ MeV.$$

The interaction potential (48) is integrable, thus, it does not necessarily require the smoothing procedure [35,88,114]. For the interaction–energy density (29) we have

$$\Phi_{33} = \int \Phi_{33}(\vec{r}) d\vec{r}, \tag{49}$$

which yields $\Phi_{33} = 4.1 \times 10^{-5}\ MeV^{-2} = 315\ MeV/fm^3$. Note that $\Phi_{33}\rho_0 = 164\ MeV$, hence $\Phi_{33}\rho_0 \approx E_0 = \rho_0^{1/3}$, from where $\Phi_{33} \approx \rho_0^{-2/3}$.

For the spectra of baryons we take

$$\varepsilon_i(k) = \sqrt{k^2 + m_i^2} + \frac{z_i}{9}(\rho - \rho_q)\Phi_{33}. \tag{50}$$

where ρ_q is the quark density and i enumerates multiquark clusters: $3q$, $6q$, $9q$ $12q$, and so on. The masses of bound clusters up to $z_i = 12$ are taken from Table 1, with the six–quark mass $m_6 = 1944\ MeV$. For $z_i \geq 15$ we use the formula $m_i \approx (z_i/3)m_3$ for the masses of heavy multiquark clusters [22].

For quarks we accept the mass $m_q = 7\ MeV$ and the degeneracy factor $\zeta_q = 12$ corresponding to spin $1/2$, $N_c = 3$, and $N_f = 2$. The bag constant $B^{1/4} = 235\ MeV$.

The results of numerical calculations [115-119] are presented in Figs.6-13. At $\Theta = 0$ and $\rho = \rho_0$, the $6q$-probability is $w_6 = 0.18$, which agrees with the estimates of the $6q$-admixture in nuclei [120]. The heavy–multiquark probabilities are always small: $w_9 < 10^{-3}$, $w_{12} < 10^{-5}$, and $w_{15} < 10^{-7}$. At zero temperature, only the Bose–condensed $6q$-clusters exist, the probabilities of heavier ones being strictly zero. Unbound quarks, at $\Theta = 0$, are absent below the density $\rho_q^{nuc} \approx 2\rho_0$ when they start appearing. This is why the characteristic

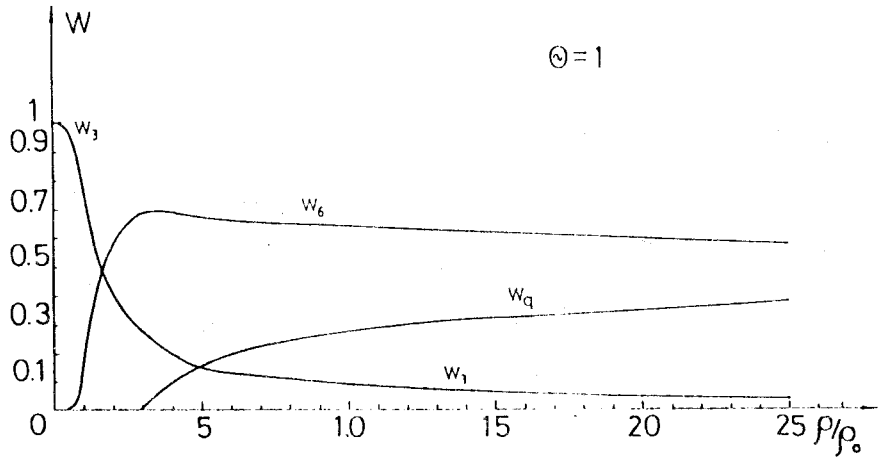

Fig.6. Nucleon, $6q$–cluster, and unbound quark probabilities as functions of the relative density at $\Theta = 0$

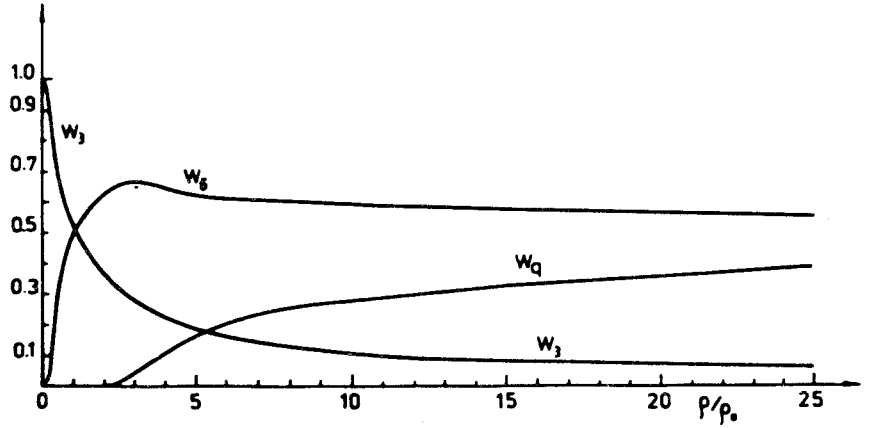

Fig.7. Probabilities of unbound quarks and of bound clusters vs. relative density at $\Theta = 30$ *MeV*

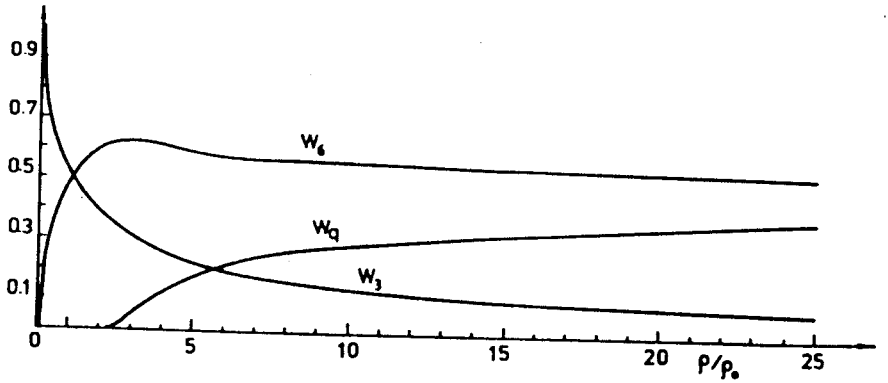

Fig.8. Cluster probabilities vs. relative density at $\Theta = 50$ *MeV*

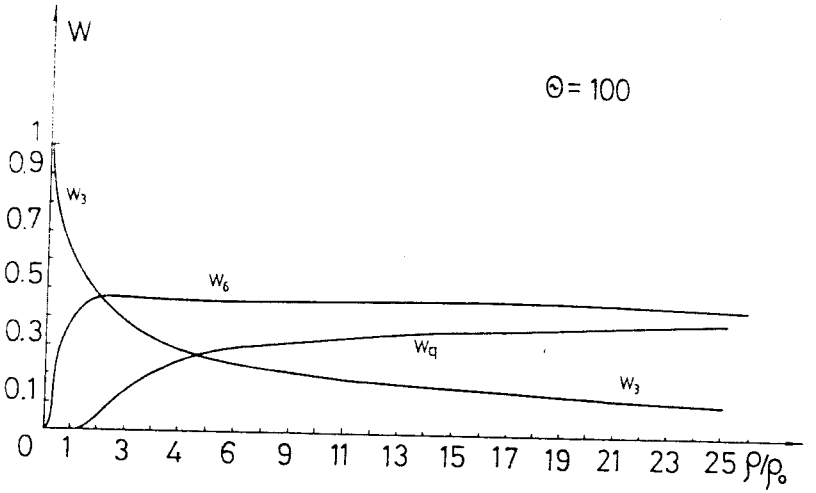

Fig.9. Cluster probabilities at $\Theta = 100$ *MeV*

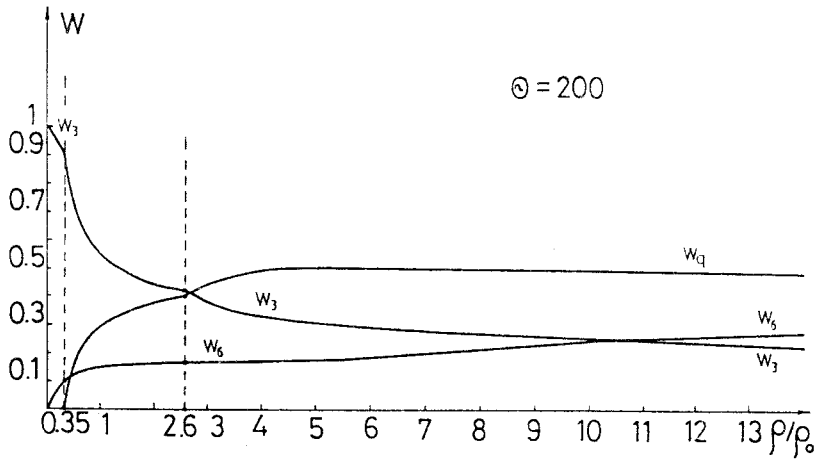

Fig.10. Cluster probabilities at $\Theta = 200$ MeV. Dashed lines show the points of first order phase transitions. Between these points the matter is a stratified gas-liquid mixture

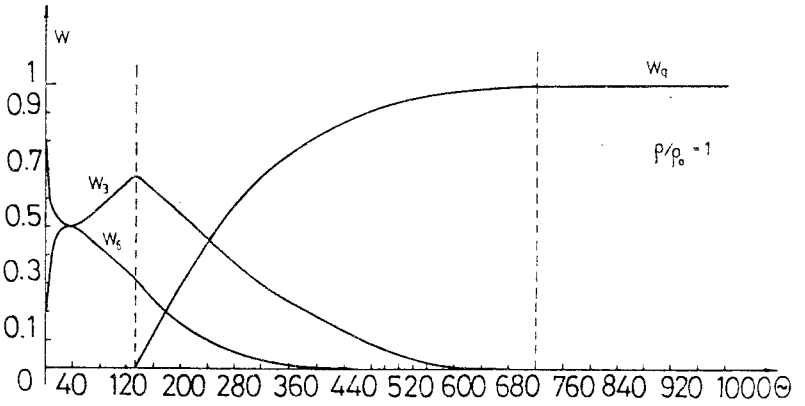

Fig.11. Nucleon, $6q$-cluster, and quark probabilities as functions of temperature in MeV at the normal density $\rho = \rho_0$

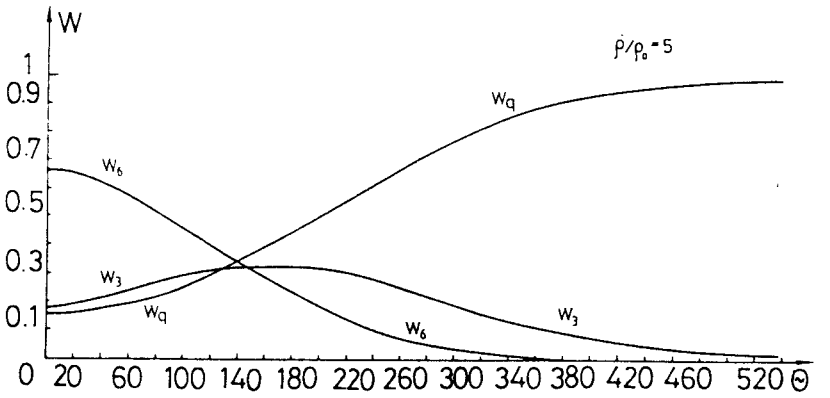

Fig.12. Cluster probabilities vs. temperature at the fixed density $\rho = 5\rho_0$

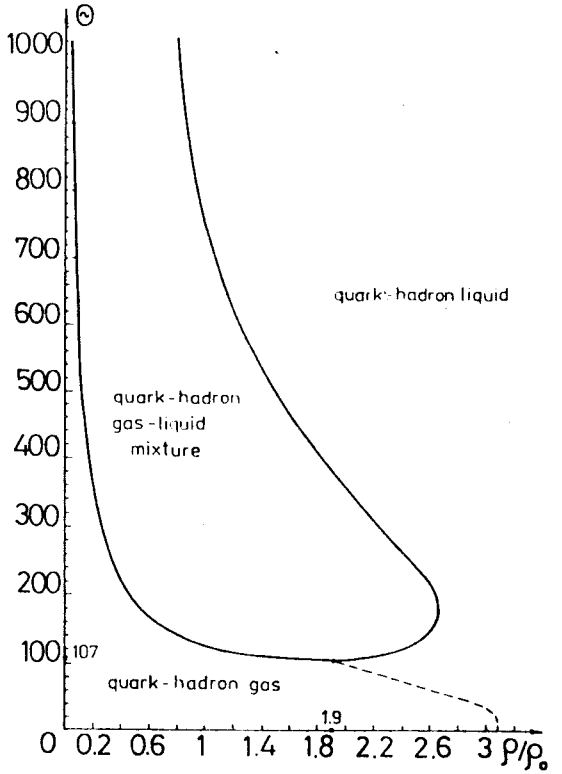

Fig.13. Phase portrait for the baryon rich quark-hadron matter. Along the dashed line the compressibility is divergent

density ρ_q^{nuc} may be called the *nucleation density*. As we see, the value of the latter agrees with the corresponding estimates from Introduction.

The stability of the quark–baryon mixture is controlled by checking the minimum of the free energy $F = \Omega + \sum_i \mu_i N_i$ whose density can be written as

$$f \equiv \frac{F}{V} = \frac{\Omega}{V} + \sum_i \mu_i \rho_i = -p + \mu\rho,$$

and also by requiring the validity of the stability conditions [54]

$$-\Theta \frac{\partial^2 f}{\partial \Theta^2} > 0, \qquad \rho \frac{\partial p}{\partial \rho} > 0.$$

The probability of unbound quarks increases, with temperature or density monotonically showing that the deconfinement is a gradual crossover but not a sharp transition. This is in agreement with numerical simulations [121] on $16^3 \times 24$ lattice, for $N_f = 2$, which has demonstrated that quark–quark correlation functions at $\Theta \approx 1.5\Theta_d$ are very similar to the zero–temperature wave functions of the corresponding particles.

12. ZERO BARYON DENSITY

The case opposite to that of the previous section is when the baryon density is zero, $n_{0B} = 0$, and all particles are generated from vacuum. Then $\mu_i = 0$. In this case, we can compare our calculations with the lattice numerical simulations that are available only for $n_B = 0$.

The spectra of gluons and quarks are again taken in the form

$$\omega_g(k) = k + \frac{B}{\rho}, \qquad \omega_q(k) = \sqrt{k^2 + m_q^2} + \frac{B}{\rho} \tag{51}$$

with the bag–motivated mean fields.

The interaction of hadrons is considered in the excluded-volume approximation. The cluster volumes $v_i = m_i v_2/m_2$, according to (45), are expressed through the volume $v_2 \equiv 4\pi r_2^3/3$ of the lightest cluster with $z_i = 2$. The bag constants for the $SU(2)$ and $SU(3)$ systems are to be different [122] with the relation $B_{SU(2)} \approx 0.4 B_{SU(3)}$.

The presentation of results is convenient to perform in relative quantities reduced to these of a reference system. The role of such a system is naturally played by the Stefan–Boltzmann quark–gluon gas. The latter, by definition, is an ensemble of free massless quarks, antiquarks, and gluons. The pressure and energy density of the Stefan–Boltzmann quark–gluon plasma are, respectively,

$$p_{SB} = p_q^{(0)} + p_{\bar{q}}^{(0)} + p_g^{(0)}, \qquad \varepsilon_{SB} = \varepsilon_q^{(0)} + \varepsilon_{\bar{q}}^{(0)} + \varepsilon_g^{(0)}, \tag{52}$$

where

$$p_i^{(0)} = \pm\Theta\zeta_i \int \ln\left[1 \pm n_i^{(0)}(k)\right] \frac{d\vec{k}}{(2\pi)^3},$$

$$\varepsilon_i^{(0)} = \zeta_i \int k n_i^{(0)}(k) \frac{d\vec{k}}{(2\pi)^3}, \tag{53}$$

the index $i = q, \bar{q}, g$ enumerates quarks, antiquarks, and gluons with the momentum distribution

$$n_i^{(0)}(k) = \{\exp[\beta(k - \mu_i)] \mp 1\}^{-1}, \tag{54}$$

in which the upper sign is for Bosons (gluons) and the lower one, for Fermions (quarks and antiquarks); the chemical potentials being

$$\mu_q = -\mu_{\bar{q}} \equiv \mu, \qquad \mu_g = 0. \tag{55}$$

Eqs. (54) and (55) permit to write down (53) as

$$p_i^{(0)} = \frac{\zeta_i}{6\pi^2} \int_0^\infty \frac{k^3 dk}{\exp[\beta(k - \mu_i)] \mp 1}, \qquad \varepsilon_i^{(0)} = 3p_i^{(0)}. \tag{56}$$

An exact integration yields

$$p_q^{(0)} + p_{\bar{q}}^{(0)} = \frac{\zeta_q}{12}\left(\frac{7\pi^2}{30}\Theta^4 + \mu^2\Theta^2 + \frac{\mu^4}{2\pi^2}\right),$$

$$p_g^{(0)} = \frac{\pi^2}{90}\zeta_g\Theta^4. \tag{57}$$

Thus, the Stefan–Boltzmann pressure is

$$p_{SB} = \frac{\pi^2}{90}\left(\zeta_g + \frac{7}{4}\zeta_q\right)\Theta^4 + \frac{\zeta_q}{12}\mu^2\Theta^2\left(1 + \frac{\mu^2}{2\pi^2\Theta^2}\right). \tag{58}$$

This is to be compared with the QCD pressure corresponding to the QCD grand potential, given in Section 3, for zero coupling $g = 0$,

$$p_{QCD} = \frac{\pi^2}{45}\left(N_c^2 - 1 + \frac{7}{4}N_f N_c\right)\Theta^4 + \frac{N_f N_c}{6}\mu^2\Theta^2\left(1 + \frac{\mu^2}{2\pi^2\Theta^2}\right). \tag{59}$$

Due to the relations for the degeneracy factor of gluons, $\zeta_g = 2 \times (N_c^2 - 1)$, and for that of quarks, $\zeta_q = 2 \times N_f \times N_c$, and antiquarks, $\zeta_q = \zeta_{\bar{q}}$, we see that (58) and (59) coincide with each other. Therefore, the Stefan–Boltzmann plasma is the asymptotic high–temperature limit of quantum chromodynamics.

The baryon density for the Stefan–Boltzmann plasma is

$$n_B \equiv \frac{1}{3}\left(\rho_q - \rho_{\bar{q}}\right) = \frac{\zeta_q}{3}\int \left[n_q(k) - n_{\bar{q}}(k)\right]\frac{d\,\vec{k}}{(2\pi)^3}. \tag{60}$$

Either calculating (60) directly or using the derivative $n_B = \partial p/\partial\mu_B$, with $\mu_B = 3\mu$ we have

$$n_B = \zeta_q \frac{\mu}{18\pi^2}\left(\mu^2 + \pi^2\Theta^2\right). \tag{61}$$

From here, one gets the equation

$$\mu^3 + \pi^2\Theta^2\mu - \frac{18\pi^2}{\zeta_q}n_B = 0 \tag{62}$$

defining $\mu = \mu(n_B)$. At zero baryon density $n_B = 0$, as is clear from (62), one has $\mu = 0$.

When the chemical potential is zero, the density of quarks becomes

$$\rho_q = \zeta_q \frac{3\Theta^3}{4\pi^2}\zeta(3) \qquad (\mu = 0), \tag{63}$$

where $\zeta(3) = 1.20206$. For gluons, the chemical potential is always zero, so their density is

$$\rho_g = \zeta_g \frac{\Theta^3}{\pi^2}\zeta(3). \tag{64}$$

Finally, for the specific heat of the Stefan–Boltzmann plasma we find

$$C_{SB} \equiv \frac{\partial\varepsilon_{SB}}{\partial\Theta} = \frac{2\pi^2}{15}\left(\zeta_g + \frac{7}{4}\zeta_q\right)\Theta^3 + \frac{1}{2}\zeta_q\mu^2\Theta^2\frac{\mu^2 - \pi^2\Theta^2}{3\mu^2 + \pi^2\Theta^2}. \tag{65}$$

The results of numerical calculations [123-125] for the mixed system, consisting of the quark–gluon plasma with the spectrum (51) and of hadrons in the excluded–volume approximation, will be presented below for three different situations.

12.1. SU(2) Quarkless System. The system consists of unbound gluons and of glueballs that are bound gluon clusters. The experimental status of glueballs is yet uncertain, though there are suggestions [126,127] to interpret a narrow resonance appearing in proton–proton collisions as a scalar glueball. Pure gluodynamics is often studied because it is easier, than the full chromodynamics, for Monte Carlo lattice simulations.

Glueball masses have been computed in the lattice gauge theory for both $SU(2)$ [43,46] as well as for $SU(3)$ [128-130] cases. The lattice results are close to the bag–model calculations [131-133]. Here we accept the glueball

masses found in the bag-model approach [132,133]. The corresponding glueball characteristics are given in Table 2. The radius r_2 of the lightest glueball with $m_2 = 960\ MeV$ is a fitting parameter which is taken as $r_2 = 1.2\ fm$. The constant B in (51) is chosen to be $B = (165\ MeV)^4$. The gluon degeneracy factor is $\zeta_g = 6$ for the $SU(2)$ case.

The results of our calculations are displayed in Figs.14-18, where the glueball probability w_G and the gluon probability w_g are defined by

$$w_G \equiv \sum_i^{glueballs} z_i \frac{\rho_i}{\rho}, \qquad w_g \equiv \frac{\rho_g}{\rho} = 1 - w_G.$$

The relative energy density is compared with the lattice data [134,135]. The reference Stefan-Boltzmann plasma here corresponds also to the quarkless case, $N_f = 0$. Deconfinement occurs at $\Theta_d = 215\ MeV$ as a second-order transition, which is in agreement with the lattice simulations.

12.2. SU(3) Quarkless System. The glueball parameters are taken from Table 2. The constant B in spectra (51) is $B = (235\ MeV)^4$. The gluon degeneracy factor for the $SU(3)$ case is $\zeta_g = 16$.

Varying the radius r_2 of the lightest glueball, we have three possibilities: (i) $r_2 < r_c$, where $r_c = 0.8 fm$; then deconfinement is a gradual crossover. (ii) $r_2 = r_c$; in this case deconfinement is a 2-order transition. (iii) $r_2 > r_c$; then 1-order transition occurs. These possibilities are illustrated in Figs.19-23, where the entropy density at $\mu_i = 0$ is $s = \beta(\varepsilon + p)$ and the reference Stefan-Boltzmann entropy density is $s_{SB} = \beta(\varepsilon_{SB} + p_{SB}) = 4\beta p_{SB}$. The relative entropy density is compared with the lattice numerical simulations [136]. The latter agrees with our results if $r_2 > r_c$, so that deconfinement becomes a 1-order transition at about $\Theta_d = 230\ MeV$.

Emphasize the importance of taking into consideration glueball interactions: When these are absent, that is $r_2 = 0$, the behaviour of the system is unphysical.

12.3. SU(3) System with Quarks. The constituents of the system are taken as follows. Consider quarks of two flavours, $q = \{u, d\}$, and the corresponding antiquarks $\bar{q} = \{\bar{u}, \bar{d}\}$ with the masses $m_q = m_{\bar{q}} = 7\ MeV$. The degeneracy factor for each pair of up and down quarks is $\zeta_q = 2 \times N_f \times N_c = 12$, and the same for antiquarks, $\zeta_{\bar{q}} = 12$. Gluons have the degeneracy factor $\zeta_g = 2 \times (N_c^2 - 1) = 16$. From the long list of the known hadrons, we include only those with the lightest masses, which mainly contribute to thermodynamics. These are unflavoured mesons (Table 3), strange mesons (Table 4) and light baryons (Table 5).

For the radius of the lightest hadron, that is of a pion, we take $r_2 = r_\pi = 0.56\ fm$. The radii of all other clusters are expresses through r_π using (45). For the mean-field parameter in (51), we accept $B^{1/4} = 210\ MeV$. The results

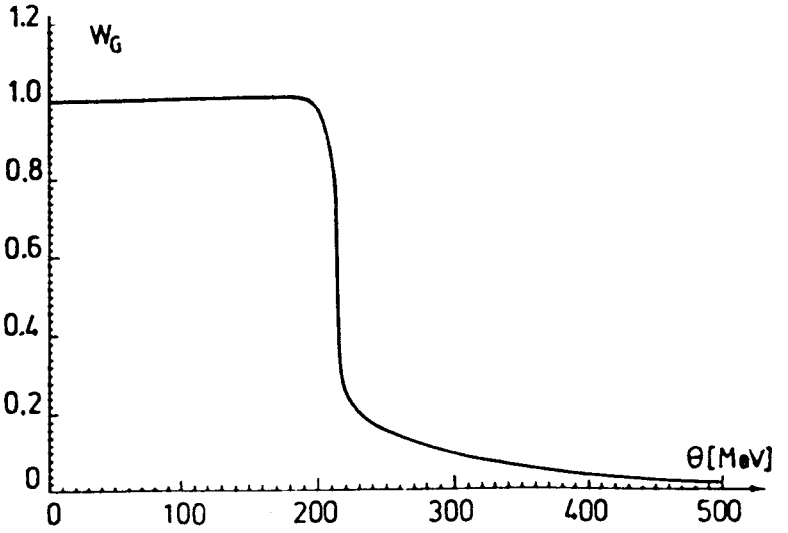

Fig.14. Glueball probability for the $SU(2)$ quarkless system as a function of temperature

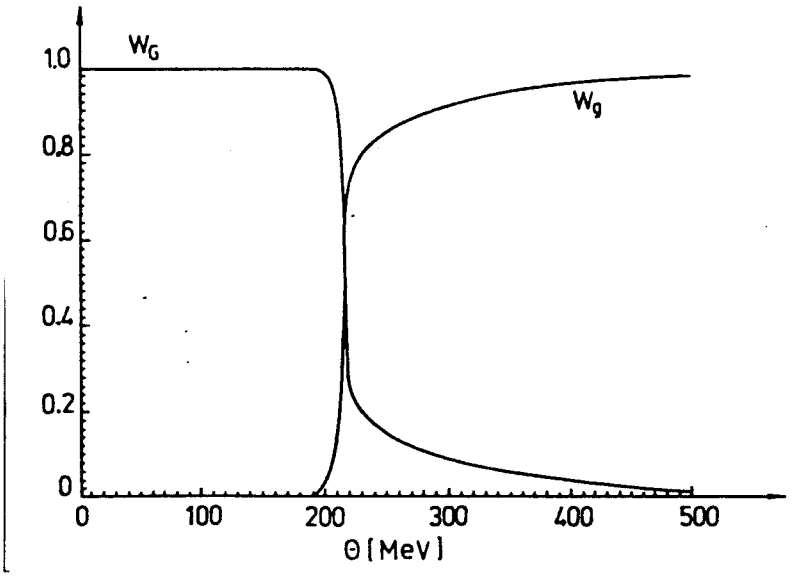

Fig.15. Comparison of glueball and gluon probabilities for the $SU(2)$ quarkless system

Table 2. Glueball parameters

Mass m_i (MeV)	Compositeness number z_i	Degeneracy factor ζ_i
960	2	6
1290	2	6
1590	2	6
1460	3	11
1800	3	39

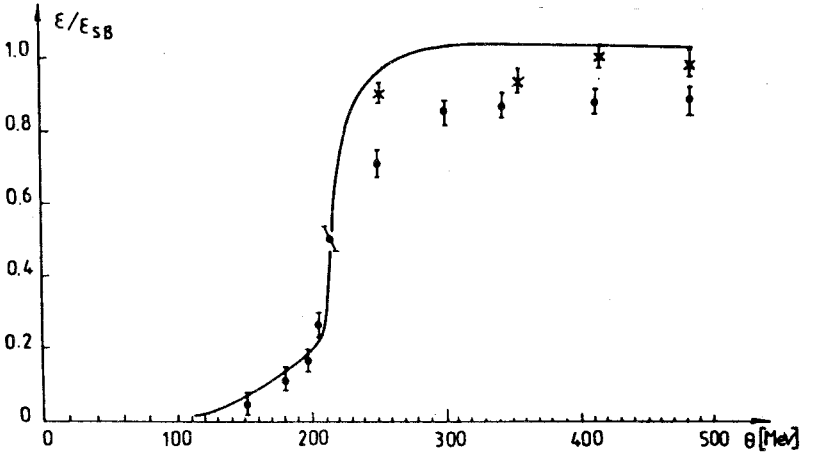

Fig.16. Relative energy density for the $SU(2)$ quarkless system (solid line) as compared with the lattice Monte Carlo data (Engels et al., 1981)

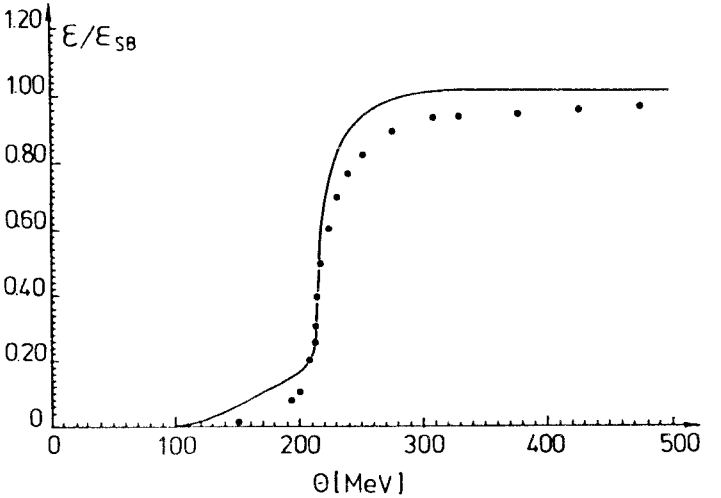

Fig.17. Relative energy density for the $SU(2)$ quarkless system (solid line) compared with the lattice numerical simulations (Engels et al., 1989)

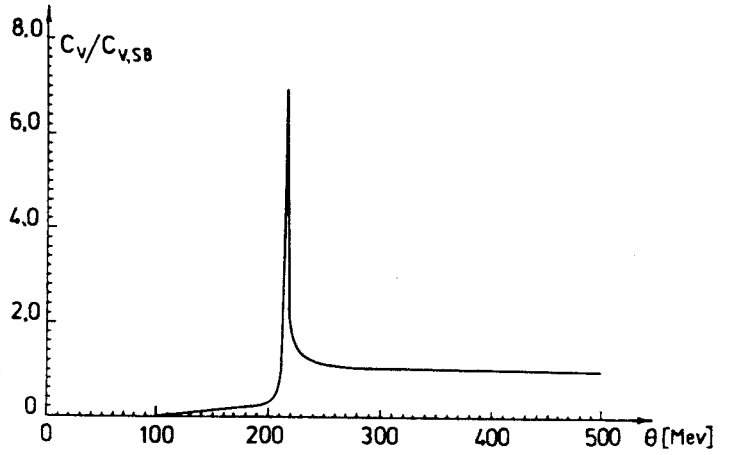

Fig.18. Reduced specific heat for the $SU(2)$ gluon-glueball mixture. At the deconfinement temperature, specific heat diverges

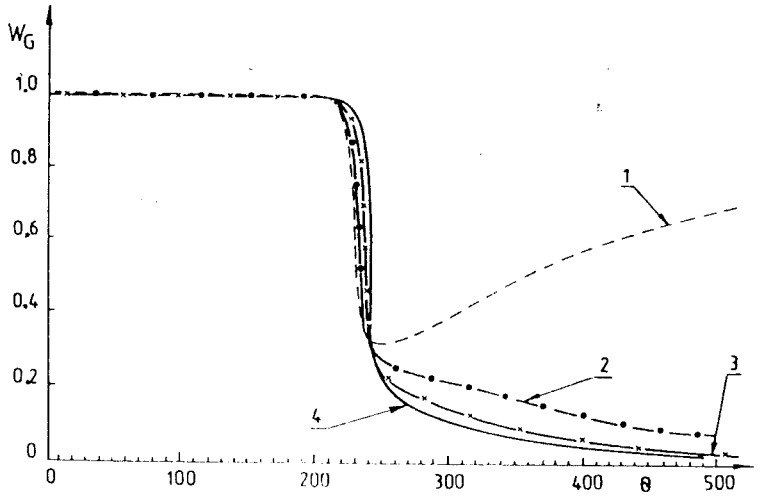

Fig.19. Glueball probability for the $SU(3)$ quarkless system at several values of the lightest glueball radius: (1) $r_2 = 0$; (2) $r_2 = 0.5$ *fm*; (3) $r_2 = 0.7$ *fm*; (4) $r_2 = 0.8$ *fm*

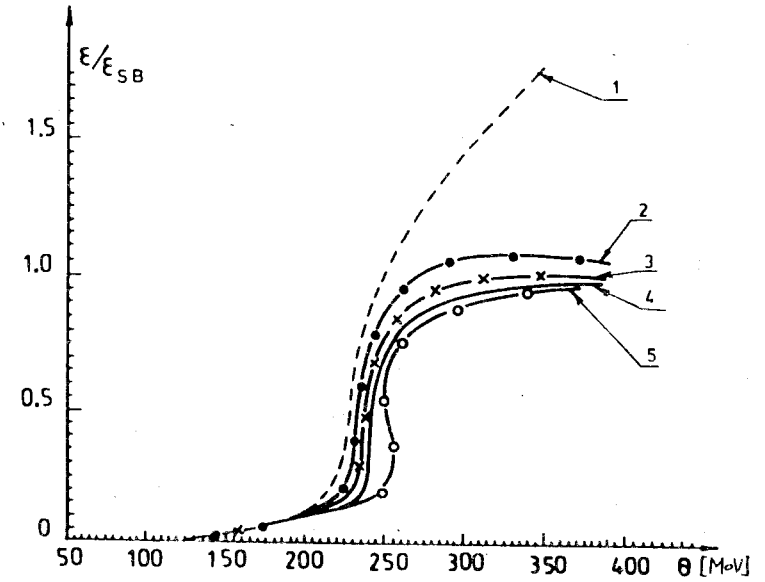

Fig.20. Relative energy density for the $SU(3)$ quarkless system at: (1) $r_2 = 0$; (2) $r_2 = 0.5$ *fm*; (3) $r_2 = 0.7$ *fm*; (4) $r_2 = 0.8$ *fm*; (5) $r_2 = 1$ *fm*

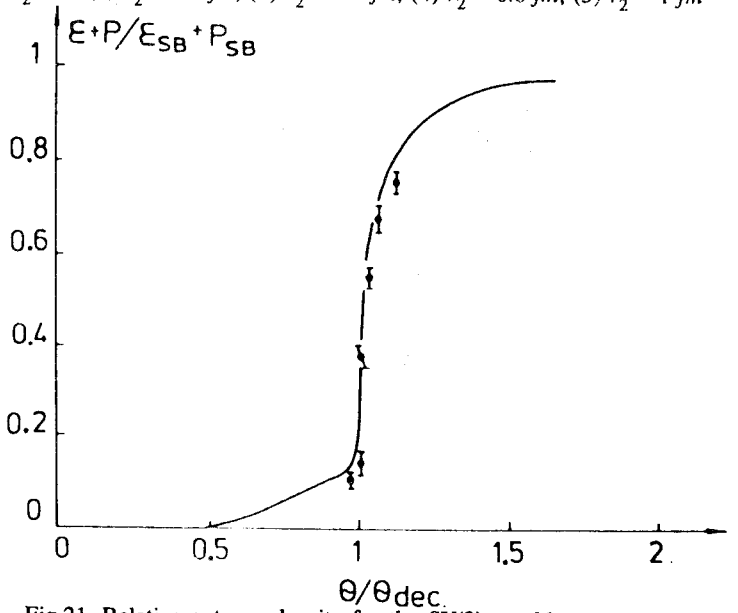

Fig.21. Relative entropy density for the $SU(3)$ quarkless system at $r_2 = 0.82$ *fm* compared with the lattice numerical data (Brown et al., 1988)

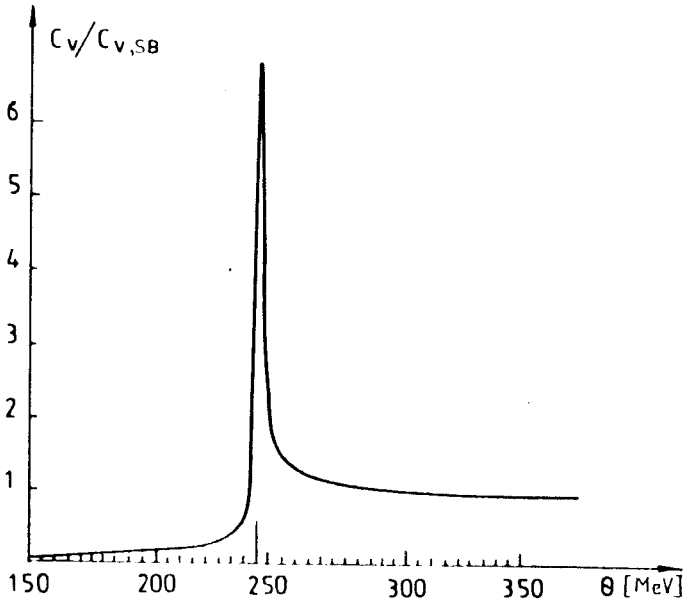

Fig.22. Reduced specific heat for the $SU(3)$ gluon-glueball mixture at $r_2 = 0.8$ *fm*

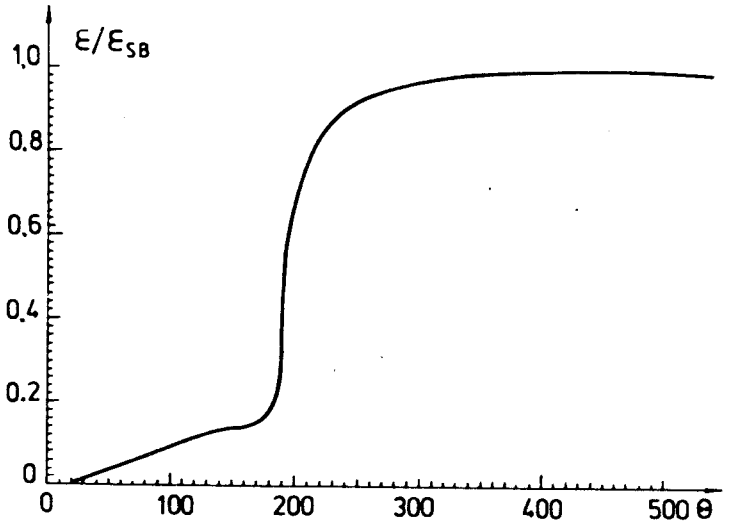

Fig.23. Relative energy density for the $SU(3)$ quarkless system at $B^{1/4} = 210$ MeV and $r_2 = 0.6$ *fm*

Table 3. Unflavoured meson parameters

Mesons	Mass m_i (MeV)	Compositeness number z_i	Degeneracy factor ζ_i
π^+	140	2	1
π^-	140	2	1
π^0	135	2	1
η	548	2	1
ρ^+	770	2	3
ρ^-	770	2	3
ρ^0	770	2	3
ω	782	2	3

Table 4. Strange meson parameters

Mesons	Mass m_i (MeV)	Compositeness number z_i	Degeneracy factor ζ_i
K^+	494	2	1
K^-	494	2	1
K^0	498	2	2
$\overline{K}^0$	498	2	2

Table 5. Baryon parameters

Baryons	Mass m_i (MeV)	Compositeness number z_i	Degeneracy factor ζ_i
N	939	3	4
$\overline{N}$	939	3	4
Δ	1232	3	16
$\overline{\Delta}$	1232	3	16

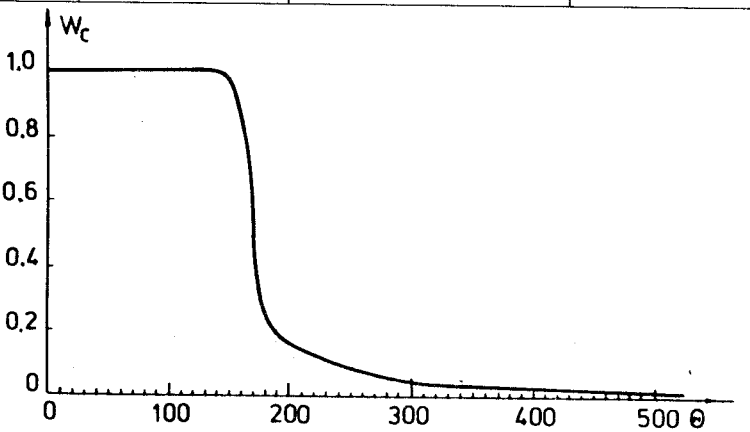

Fig.24. Hadron cluster probability for the mixture of quark-gluon plasma and hadrons at zero baryon density

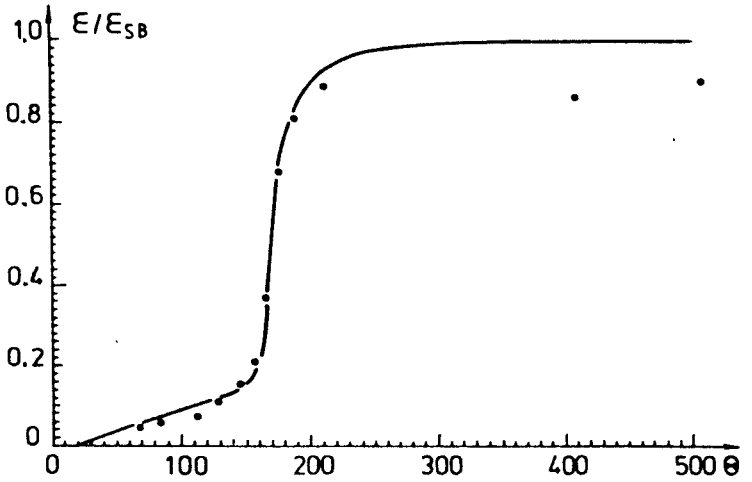

Fig.25. Relative energy density for the mixture compared with the lattice numerical calculations (Çelik et al., 1985)

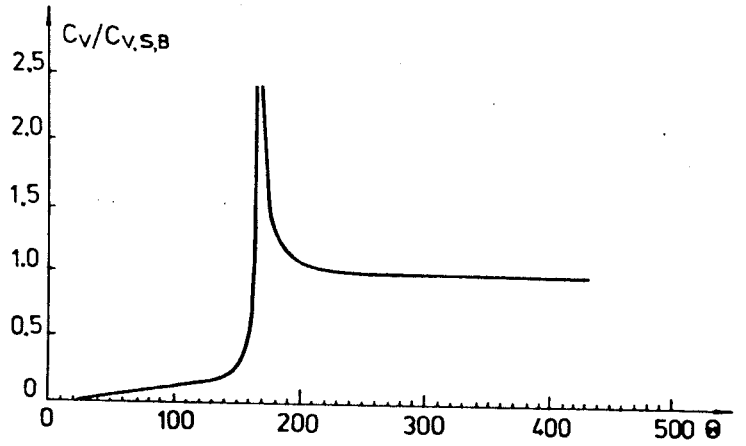

Fig.26. Reduced specific heat for the mixture of quark-gluon plasma and hadrons at zero baryon density

of calculations are shown in Figs.24-26, where the hadron cluster probability is defined as

$$w_c \equiv \sum_i^{clusters} z_i \frac{\rho_i}{\rho} .$$

Deconfinement is found to be rather a continuous crossover-like transition at $\Theta_d = 166 MeV$, which is close to lattice data [137].

13. THERMODYNAMIC RESTRICTION RULE

Invoking this or that approximation, one gets an effective thermodynamic potential, for instance, an effective grand potential $\Omega = \Omega(\Theta, V, \mu, \varphi)$, involving some auxiliary functions $\varphi = \{\varphi_j\}$ depending on thermodynamics parameters, temperature Θ, volume V, and a set $\mu = \{\mu_i\}$ of chemical potentials. Thus, effective spectra in (51) contain the mean field $\varphi \equiv B/\rho$. In the excluded-volume approximation, the free volume of the system is factored with the quantity $\xi = 1 - \sum_i \rho_i v_i$, as is seen from (42). Both ρ and ρ_i are functions of Θ, V, μ. In the cut-off model of Section 5, the effective cut-off momentum k_0 is a function of Θ.

Effective thermodynamic potentials are to be handled with great caution. Really, if one calculates, e.g., the pressure

$$p = -\frac{\partial \Omega}{\partial V} = -\frac{\Omega}{V} = \frac{\Theta}{V} \ln \mathrm{Tr}\, e^{-\beta H} \tag{66}$$

in two different ways, as the derivative $(-\partial\Omega/\partial V)$ or as the ratio $(-\Omega/V)$, then the answers can be different when Ω includes auxiliary functions depending on V. This would mean that the relation (66) breaks. The same concerns the energy density, entropy density, and the cluster densities, respectively,

$$\varepsilon = \Theta \frac{\partial p}{\partial \Theta} - p + \sum_i \mu_i \rho_i = \frac{1}{V} \langle \hat{E} \rangle ,$$

$$s = \frac{\partial p}{\partial \Theta} = \beta \left(\varepsilon + p - \sum_i \mu_i \rho_i \right) ,$$

$$\rho_i = \frac{\partial p}{\mu_i} = \frac{1}{V} \langle \hat{N}_i \rangle , \tag{67}$$

which may be defined in two ways, as first derivatives of pressure or as the corresponding statistical averages. Definition (67) can also become broken when

auxiliary functions depend on thermodynamic variables. This kind of inconsistency occurs as well for the second derivatives, such as the specific heat

$$C_V = \frac{\partial \varepsilon}{\partial \Theta} = \frac{\beta^2}{V}\left(\langle \hat{E}^2 \rangle - \langle \hat{E} \rangle^2\right) \tag{68}$$

or the isothermic compressibility

$$\kappa_T = -\frac{1}{V}\left(\frac{\partial p}{\partial V}\right)^{-1} = \frac{\beta}{\rho^2 V}\left(\langle \hat{N}^2 \rangle - \langle \hat{N} \rangle^2\right). \tag{69}$$

These inconsistencies in defining thermodynamic characteristics in two ways, thermodynamic and statistical, of course, are not pleasant. Moreover, the difference between these two ways is not only quantitative, but can also become drastic, especially for systems with phase transitions. It is even possible to give examples when the definition through the derivatives yields unphysical divergencies in the energy and entropy densities at the phase transition point. This, for instance, happens, as is easy to check, for a pure gluon model in the effective spectrum approximation.

The simplest procedure for avoiding the described troubles can be formulated as follows. Let x be any of the thermodynamic variables Θ, V or μ. If Ω is an effective grand potential including auxiliary functions depending on these thermodynamic variables, then

$$\frac{\partial \Omega}{\partial x} = \left(\frac{\partial \Omega}{\partial x}\right)_{\varphi} + \frac{\partial \Omega}{\partial \varphi} \cdot \frac{\partial \varphi}{\partial x}.$$

It is just the second term here which causes all unpleasant problems. So, the decision is evident: the derivatives $\partial\Omega/\partial x$ are to be understood in the restricted sense as

$$\frac{\partial \Omega}{\partial x} \to \left(\frac{\partial \Omega}{\partial x}\right)_{\varphi}. \tag{70}$$

The consent (70) may be called the *thermodynamic restriction rule*. We always employ this rule dealing with effective thermodynamic potentials. If the derivatives in (66)-(69) are understood in the sense of (70), then both ways of calculating thermodynamic characteristics yield the same answers.

Although with the restriction rule (70) we avoid the appearance of spurious terms so that all relations (66)-(69) become self–consistent, another problem can arise when dealing with effective thermodynamic potentials. This is the occurrence of instability regions around a transition point, where either the specific heat C_V or the isothermic compressibility κ_T are negative. Below we illustrate this for the $SU(3)$ quarkless system of subsection 12.2 with the mean–field parameter $B = (225\ MeV)^4$. The results are shown in Figs.27-34. The

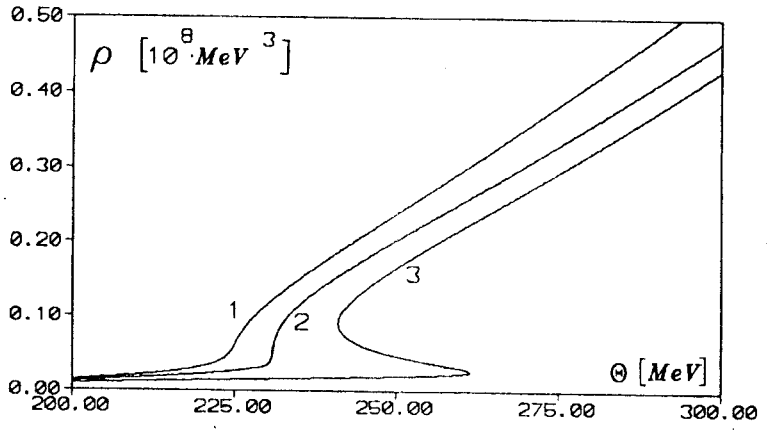

Fig.27. Total density as a function of temperature for the $SU(3)$ gluon-glueball mixture at different values of the lightest glueball radius: (1) $r_2 = 0.6$ *fm*; (2) $r_2 = 0.8$ *fm*; (3) $r_2 = 1$ *fm*

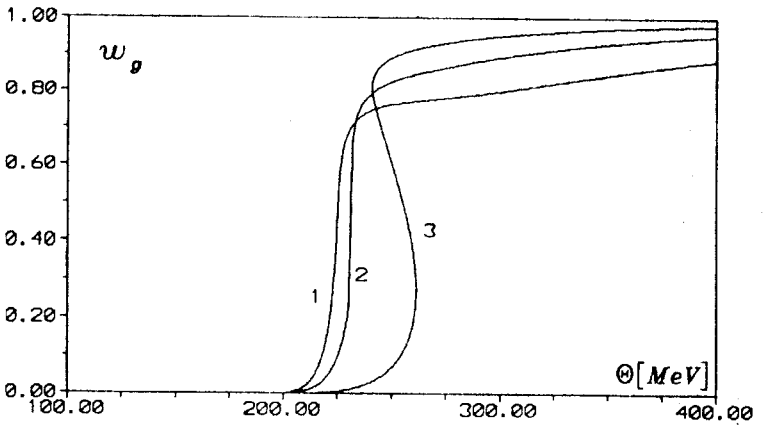

Fig.28. Gluon probability vs. temperature for the values of r_2 as in Fig.27

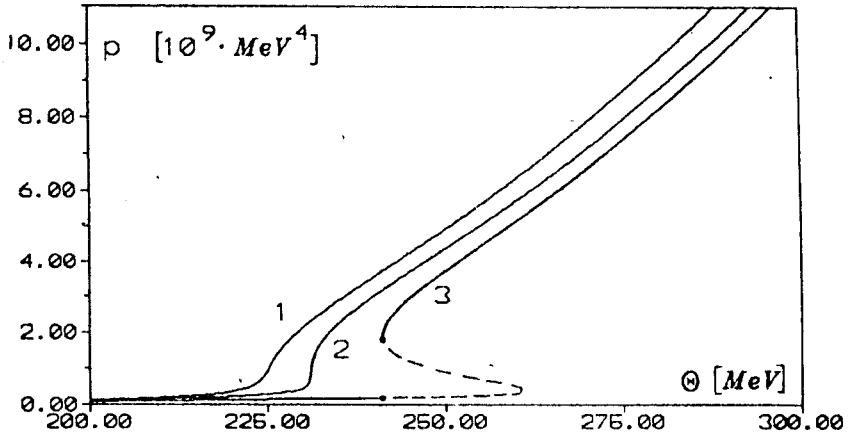

Fig.29. Pressure of the gluon-glueball mixture vs. temperature for the same values of r_2 as in Fig.27

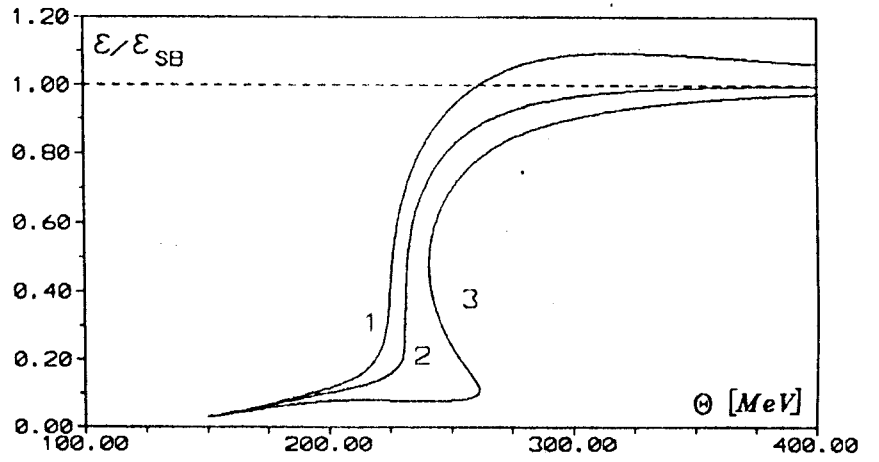

Fig.30. Relative energy of the mixture for the values of r_2 as in Fig.27

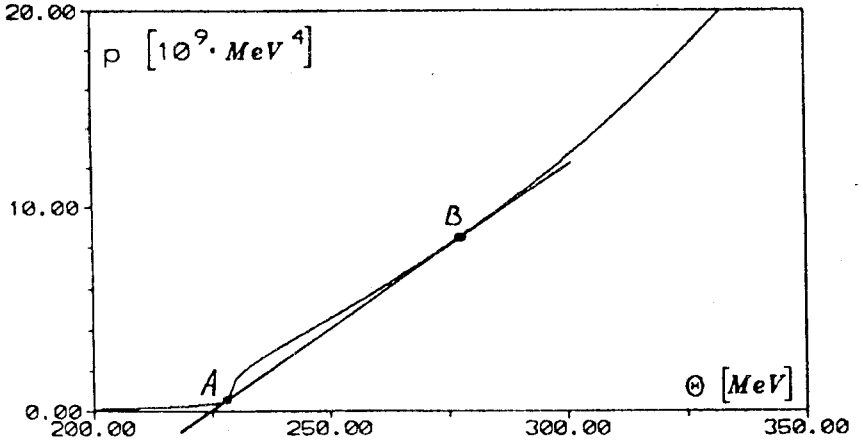

Fig.31. Smoothing of pressure in the unstable crossover region at $r_2 = 0.7$ *fm*

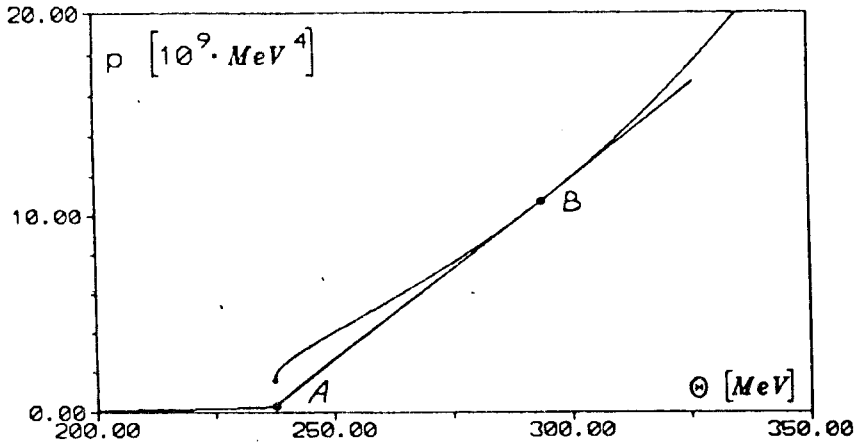

Fig.32. Smoothing of pressure in the region of first-order phase transition at $r_2 = 1$ *fm*

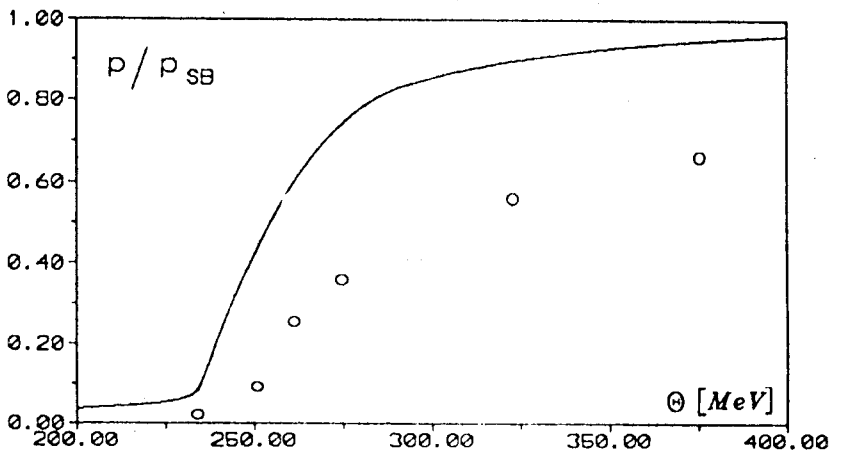

Fig.33. Relative smoothed pressure for the gluon-glueball system at $r_2 = 0.9$ *fm* (solid line) as compared with the lattice simulation data (Engels, 1991)

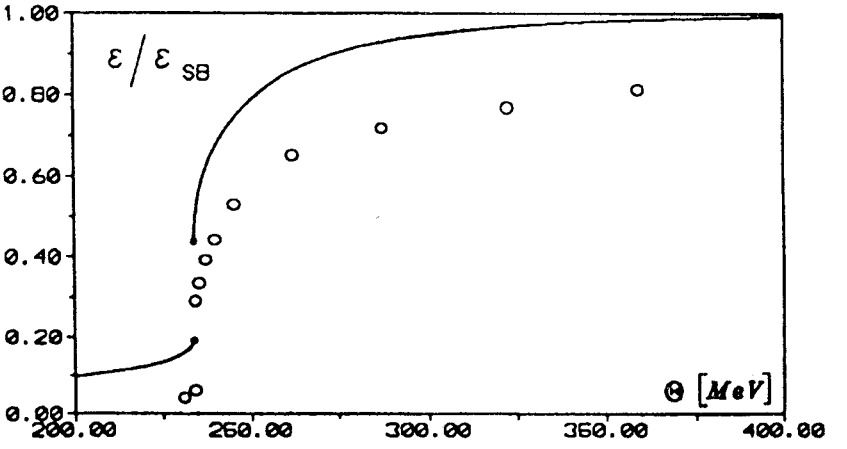

Fig.34. Relative smoothed energy at $r_2 = 0.9$ *fm* (solid line) compared with the lattice data (Engels, 1991)

unstable solutions appearing in the vicinity of transition points are related to the loss of convexity of pressure. To restore the convexity, we may resort to the Maxwell construction smoothing the corresponding thermodynamic potential [138]. Such a smoothing is shown in Figs.31 and 32. The behaviour of the resulting pressure and energy density is in a reasonable agreement with lattice simulations [50]. Nevertheless, a slight dissatisfaction rests with the fact that instability regions occur not only around a 1-order transition, where this would be more or less natural, but also in the vicinity of a continuous transition.

Instead of relying on the restriction rule (70), it would seem rational to define an effective thermodynamic potential, from the beginning, in such a way that all necessary thermodynamic relations would be automatically valid. This goal can be achieved [139] by redefining thermodynamic characteristics with the help of the shifts of the chemical potentials, $\mu_i \to \mu_i - u_i$, pressure, $p \to p + p'$, energy density, $\varepsilon \to \varepsilon + \varepsilon'$, and entropy density, $s \to s + s'$ requiring that the shifting functions u_i, p', ε', and s' guarantee the validity of (66) and (67). The latter then are named the self–consistency conditions [139]. In this case, (66) and (67) is a system of nonlinear differential equations, for the functions u_i, p', ε' and s', in partial derivatives with respect to the variables Θ, V and μ_i. Such a system has no unique solution, especially when boundary conditions are not known. To extract a solution from the self–consistency equations needs several additional heuristic assumptions and fitting parameters. Some simplification comes from the guideline prescribed by mean–field approximations [140-142].

14. PRINCIPLE OF STATISTICAL CORRECTNESS

In this section we present a new principle allowing a correct construction of effective thermodynamic potentials. This principle, as compared to the self–consistency conditions, is: (i) more general, yielding these conditions but not conversely; (ii) much simpler to deal with; (iii) unambiguous, providing a unique solution.

Let an effective thermodynamic potential $\Omega_{eff} = \Omega_{eff}(\varphi)$ include a set $\varphi = \{\varphi_i(x)\}$ of auxiliary functions depending on arbitrary variables x. The latter, in particular, may incorporate space and thermodynamic variables. First of all, it is necessary to understand that not any effective potential can have sense, however reasonable it may look. Each thermodynamic potential, to be accepted as such, must have the properties formulated below.

Property 1. **Statistical Representability**:

An effective thermodynamic potential Ω_{eff} represents an equilibrium statistical system if and only if it has the Gibbs form

$$\Omega_{eff}(\varphi) = \Omega\left[H_{eff}(\varphi)\right], \tag{71}$$

where

$$\Omega[H] \equiv -\Theta \ln \mathrm{Tr}\, e^{-\beta H}, \tag{72}$$

depending on auxiliary functions only through an effective Hamiltonian $H_{eff} = H_{eff}(\varphi)$. Such a thermodynamic potential is called *statistically representable.*

In this way, if one invents an effective thermodynamic potential, even pronouncing seemingly plausible words, this does not mean that the invented potential describes some statistical system. If the potential is not statistically representable, it represents no equilibrium statistical system. For example, a thermodynamic potential in the excluded–volume approximation is not statistically representable. Although the latter approximation may occasionally give a reasonable description, but in general it is not trustworthy. The excluded–volume approximation may be used, because of its simplicity, as a first attempt of understanding the qualitative behaviour of a system, but it should be always followed by a more reliable approximation.

Property 2. **Thermodynamic Equivalence**:

A statistical system described by a given Hamiltonian H_{giv} is thermodynamically equivalent to a system modeled by an effective Hamiltonian H_{eff} if and only if their thermodynamic potentials are statistically representable,

$$\Omega_{giv} = \Omega[H_{giv}], \qquad \Omega_{eff} = \Omega[H_{eff}], \tag{73}$$

and are equal to each other,

$$\Omega[H_{giv}] = \Omega[H_{eff}]. \tag{74}$$

The corresponding Hamiltonians are called *thermodynamically equivalent.*

For the case of infinite matter, such as nuclear matter, the equality (74) can be softened by requiring the validity of the asymptotic, in the thermodynamic limit, equality

$$\lim_{V\to\infty} \frac{1}{V} \left(\Omega[H_{giv}] - \Omega[H_{eff}]\right) = 0.$$

Property 3. **Statistical Equilibrium**:

The necessary condition for an equilibrium statistical system modelled by an effective Hamiltonian $H_{eff}(\varphi)$ to be thermodynamically equivalent to a given statistical system with H_{giv} is the equilibrium condition

$$\left\langle \frac{\delta}{\delta\varphi} H_{eff}(\varphi) \right\rangle = 0, \tag{75}$$

where the variation over φ implies a set of variations with respect to each φ_i and

$$\langle \hat{A} \rangle \equiv \frac{\mathrm{Tr}\hat{A}\exp(-\beta H_{eff})}{\mathrm{Tr}\exp(-\beta H_{eff})}.$$

The proof of (75) is straightforward basing on the statistical representability (71), thermodynamic equivalence (74) and the fact that Ω_{giv} does not depend on φ.

Now we can formulate the central notion:

Principle of Statistical Correctness:

An effective thermodynamic potential is statistically correct if it is statistically representable with an effective Hamiltonian satisfying the condition (75) of statistical equilibrium.

As is evident, the self–consistency conditions for the first-order derivatives (66) and (67) immediately follow from (75). Moreover, the self–consistency conditions for the second–order derivatives (68) and (69) also follow from (75) as well as such conditions for the derivatives of arbitrary order. While if one finds the shifting functions from the first–order self–consistency conditions (66) and (67), the second–order conditions (68) and (69) are not necessarily fulfilled.

We shall also say that an effective Hamiltonian is statistically correct if it satisfies (75). The same can be said about an approximation leading to a statistically correct Hamiltonian. For instance, the correlated mean–field approximation of Section 9, involving conditions (26) or (27), or (31), is statistically correct.

15. CLUSTERING QUARK–HADRON MATTER

To obtain a statistically correct description of the quark–gluon plasma clustering into hadron states, let us use the correlated mean–field approximation [35] leading to the Hamiltonian

$$H = \sum_i H_i + CV,$$

$$H_i = \sum_k \omega_i(k) a_i^\dagger(\vec{k}) a_i(\vec{k}),$$

$$\omega_i(k) = \sqrt{k^2 + m_i^2} + U_i - \mu_i \qquad (76)$$

discussed in Section 9.

Consider the case of the conserved baryon number $N_B = \sum_i N_i^B$ with $N_i^B \equiv B_i N_i$, where B_i is the baryon number of an i-cluster. For an equilibrium system, the relation

$$\mu_i = B_i \mu_B \tag{77}$$

holds between the chemical potential μ_i and the baryon potential μ_B. The latter may be defined as a function $\mu_B(n_B)$ of the baryon density

$$n_B \equiv \frac{N_B}{V} = \sum_i B_i \rho_i. \tag{78}$$

The index i enumerates the constituents. The total set $\{i\}$ of these indices consists of two different groups, $\{i\} = \{i\}_{pl} \bigcup \{i\}_{cl}$. The first group $\{i\}_{pl}$ corresponds to the plasma constituents, quarks, antiquarks, and gluons, which are elementary particles, thus, having the compositeness number $z_i = 1$. The second group $\{i\}_{cl}$ enumerates hadron clusters that are bound states with compositeness number $z_i \geq 2$. Respectively, the total density of matter

$$\rho = \sum_i z_i \rho_i = \rho_{pl} + \rho_{cl}, \tag{79}$$

consists of two terms

$$\rho_{pl} = \sum_{\{i\}_{pl}} \rho_i, \qquad \rho_{cl} = \sum_{\{i\}_{cl}} z_i \rho_i$$

corresponding to the plasma density ρ_{pl} and the cluster density ρ_{cl}.

Define the plasma mean fields U_i, when $i \in \{i\}_{pl}$, as

$$U_i = U(\rho) = \rho \int V(r) s(r) d\vec{r}, \tag{80}$$

where $V(r)$ is a confining potential and $s(r)$, screening function. Before substituting into (80) a concrete confining potential, let us emphasize the general properties which the plasma mean field $U(\rho)$ must satisfy to. These properties are

$$\begin{aligned} &U(\rho) \to \infty \qquad (\rho \to 0), \\ &U(\rho) \to 0 \qquad (\rho \to \infty). \end{aligned} \tag{81}$$

The upper line in (81) means that quarks and gluons cannot exist as unbound particles at low density, that is, the colour confinement must occur as $\rho \to 0$. Or one may say that quarks and gluons cannot exist as free particles outside dense nuclear matter. The lower line in (81) reflects the phenomenon of asymptotic freedom.

There are different types of confining potentials, linear, quadratic, logarithmic, and with noninteger powers. For example, the interaction between a heavy quark and its antiquark is usually taken in the form of the Cornell potential [143,144] with the linear confining term. This form of the potential is confirmed by QCD calculations [145] and by lattice simulations [146]. The quadratic confining potential is also quite popular [77,80,91]. In addition, the intensity of mutual interactions between three plasma constituents, quarks, antiquarks, and gluons, is different [145,147]. The confining potential $V(r)$ in (80) is assumed to be an averaged potential of the form

$$V(r) = Ar^{\nu} \qquad (0 \leq \nu \leq 2). \tag{82}$$

The screening function $s(r) = c(r/a)$ is usually [91] scaled with the mean interparticle distance $a \equiv \rho^{-1/3}$. Therefore, the plasma mean field (80) with the confining potential (82) can be written as

$$U(\rho) = J^{1+\nu}\rho^{-1/3}, \tag{83}$$

where

$$J^{1+\nu} \equiv 4\pi A \int_0^{\infty} c(x)x^{2+\nu}dx.$$

We can calculate the constant J if A and $c(x)$ are known. Alternatively, we may treat J as a free parameter. The value of J can be estimated as follows. Accept that at the normal quark density ρ_0 the plasma mean field (83) becomes

$$U(\rho_0) = 3E_0 = 3\rho_0^{1/3}, \tag{84}$$

where the factor 3 stands for the three plasma constituents. Then from (83) and (84) we obtain

$$J = 3^{1/(1+\nu)}\rho_0^{1/3}. \tag{85}$$

Thus, for the linear confinement, $\nu = 1$, we get $J = 272\ MeV$, while for the quadratic confinement, $\nu = 2$, we have $J = 226\ MeV$.

For the mean field of an i-cluster we may write

$$U_i = \sum_{\{j\}_{cl}} \Phi_{ij}\rho_j + z_i\left[U(\rho) - U(\rho_{cl})\right], \tag{86}$$

where the first term describes the interaction of the given cluster with other clusters, and the second term corresponds to the interaction of this cluster with the quark–gluon plasma. The interaction potentials between clusters can be scaled according to (20), which permits to express the interaction integrals (29) through one scaling integral as

$$\Phi_{ij} = z_i z_j \Phi. \tag{87}$$

Taking into account (83) and (87) reduces (86) to

$$U_i = z_i \Phi \rho_{cl} + z_i J^{1+\nu} \left(\rho^{-\nu/3} - \rho_{cl}^{-\nu/3} \right) . \tag{88}$$

In the effective Hamiltonian (76) with the mean fields (83) and (88) the role of auxiliary functions is played by the densities ρ and ρ_{cl} . So, for the equilibrium conditions (75) we have

$$\left\langle \frac{\partial H}{\partial \rho} \right\rangle = 0, \qquad \left\langle \frac{\partial H}{\partial \rho_{cl}} \right\rangle = 0. \tag{89}$$

From (89) we have two variational equations of the type (31), whose solution, up to a constant, is easy to find:

$$C = \frac{\nu}{3-\nu} J^{1+\nu} \left(\rho^{1-\nu/3} - \rho_{cl}^{1-\nu/3} \right) - \frac{1}{2} \Phi \rho_{cl}^2 . \tag{90}$$

In this way, the effective Hamiltonian is completely defined and we can pass to particular calculations.

15.1. Pure Gluon System. Imagine an extreme situation when only gluons can exist. This case may be obtained from the general model by putting all degeneracy factors zero except that of gluons, $\zeta_g \neq 0$. Then $\rho = \rho_g$ and $\rho_{cl} = 0$. Employing the Boltzmann approximation, we find [148] that there occurs a first order transition vacuum–gluon plasma at

$$\Theta_d = J \left[\frac{\nu}{3-\nu} \exp \left(1 - \frac{\nu}{3} \right) \left(\frac{\pi^2}{\zeta_g} \right)^{\nu/3} \right]^{1/(1+\nu)} .$$

Below Θ_d there is exactly vacuum, empty space, with zero energy density $\varepsilon = 0$. Gluons appear at Θ_d with a jump. The relative latent heat at Θ_d is

$$\frac{\Delta \varepsilon_d}{\varepsilon_{SB}} = \frac{1+\nu}{\nu} \exp \left(1 - \frac{3}{\nu} \right) .$$

The degeneracy of gluons for the $SU(3)$ case is $\zeta = 16$. For the linear comfinement with $\nu = 1$, we get $\Theta_d = 248\ MeV$ and $\Delta \varepsilon_d / \varepsilon_{SB} = 0.27$. For the harmonic confinement, when $\nu = 2$, the vacuum–gluon transition happens at a higher temperature $\Theta_d = 285\ MeV$ and the latent heat is larger, $\Delta \varepsilon_d / \varepsilon_{SB} = 0.91$.

15.2. SU(2) Gluon–Glueball System. The gluon degeneracy factor for the $SU(2)$ case is $\zeta = 6$. As the scaling integral we take $\Phi = \Phi_{22}/4$. So that the interactions between glueballs are found from (87). We consider the glueballs listed in Table 2. There are two fitting parameters for which we accept

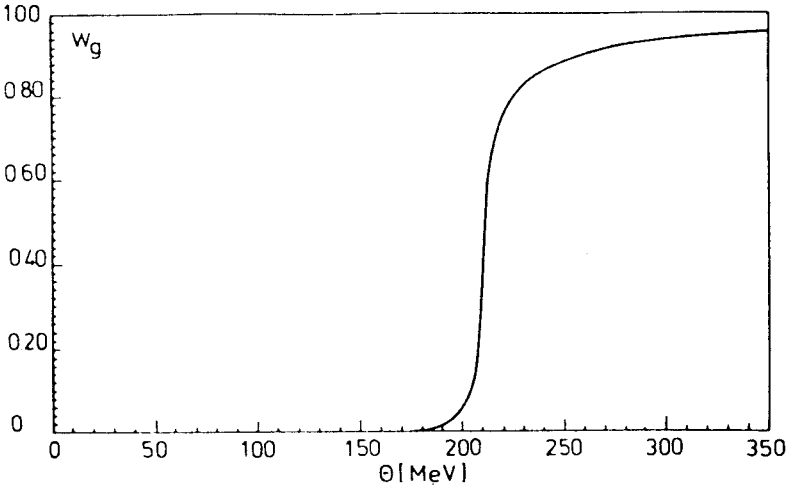

Fig.35. Gluon probability for the corrected $SU(2)$ quarkless model

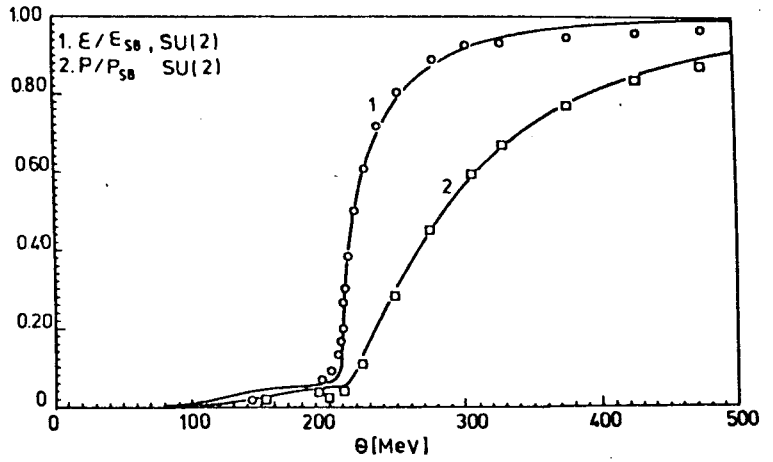

Fig.36. Relative energy and pressure for the corrected $SU(2)$ gluon-glueball model. Circles and squares are lattice simulation data (Engels, 1989)

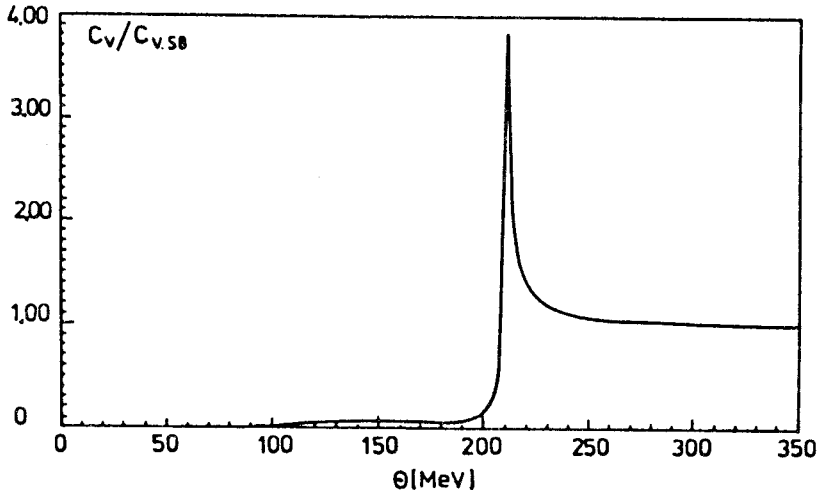

Fig.37. Reduced specific heat for the corrected $SU(2)$ quarkless model

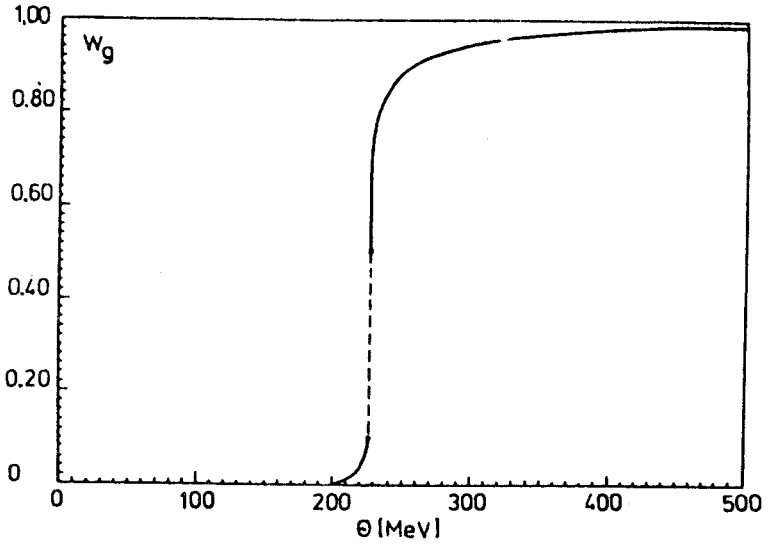

Fig.38. Gluon probability for the corrected $SU(3)$ gluon-glueball model

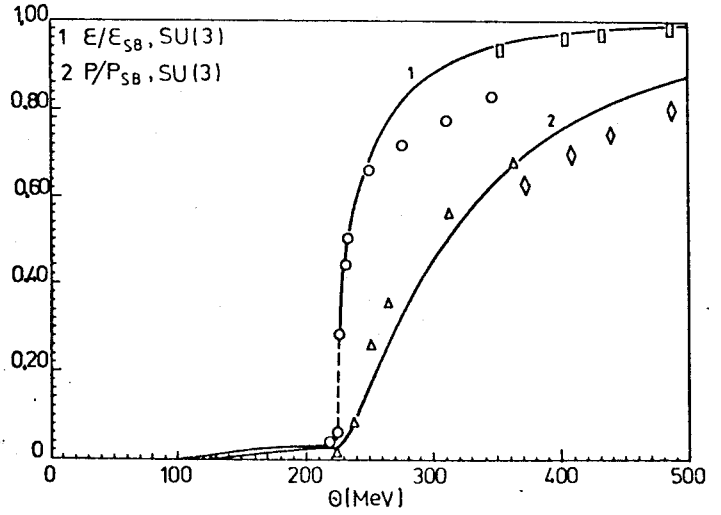

Fig.39. Relative energy and pressure for the corrected $SU(3)$ quarkless model compared with the lattice Monte Carlo calculations (Brown et al., 1988; Karsch, 1989; Engels, 1991; Petersson, 1991)

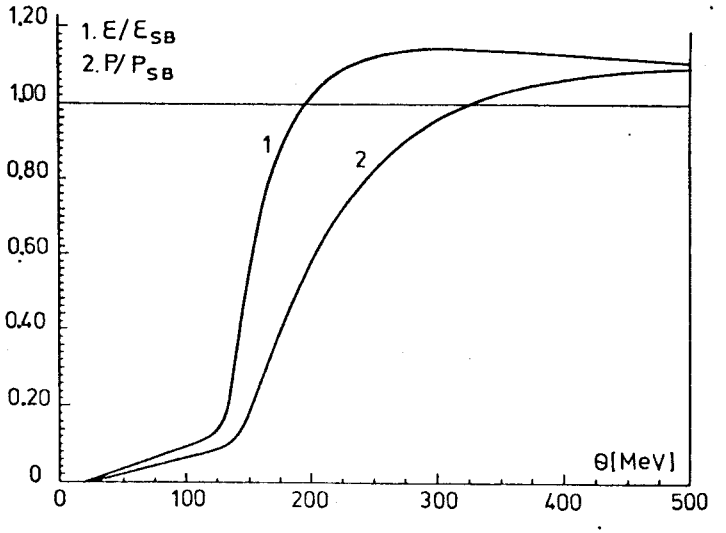

Fig.40. Relative energy and pressure for the mixed quark-gluon-meson system

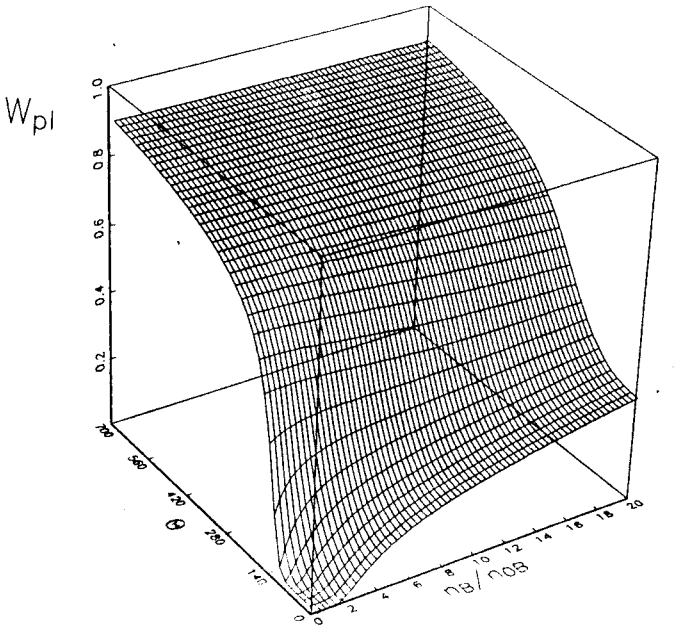

Fig.41. Quark-gluon plasma probability on the temperature-baryon density plane

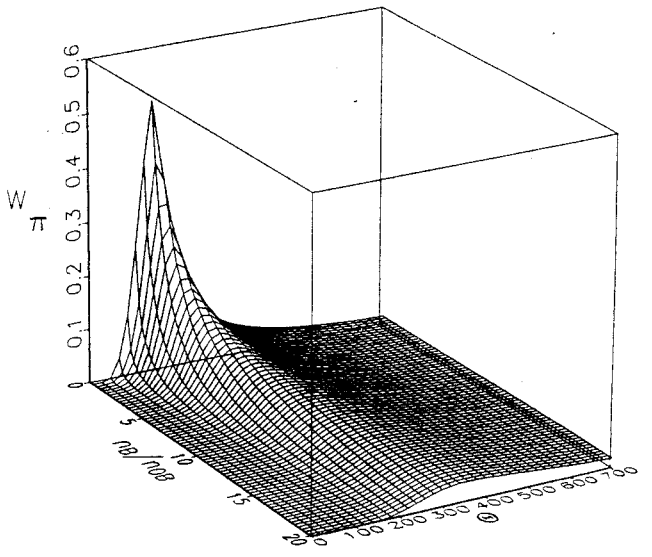

Fig.42. The probability of π-mesons

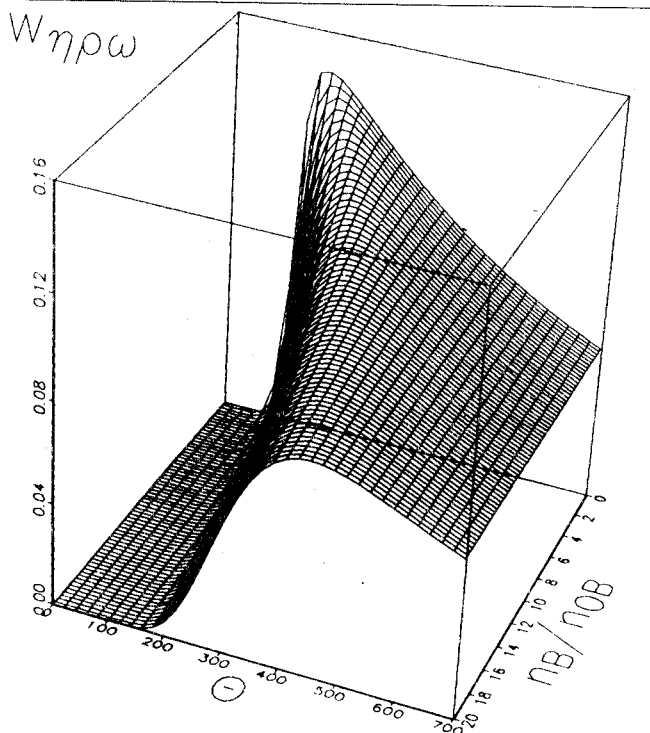

Fig.43. The total probability of η-, ρ-, and ω-mesons

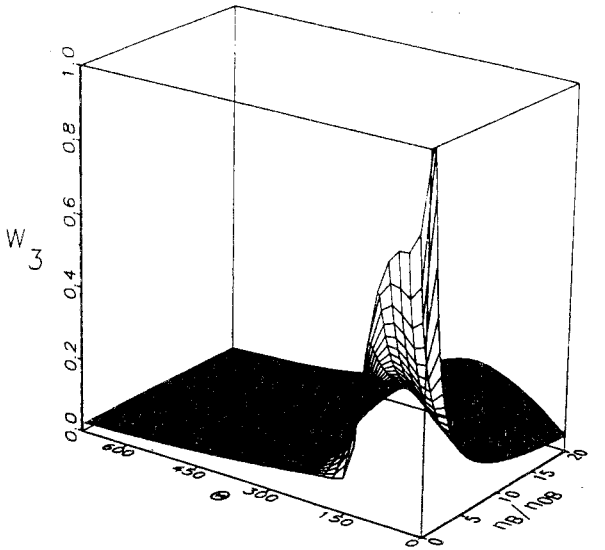

Fig.44. Nucleon probability

Fig.45. The probability of six-quark clusters

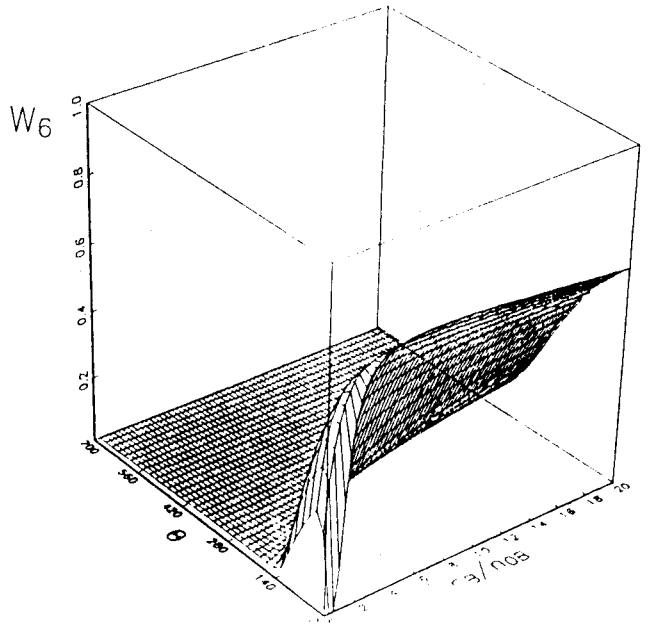

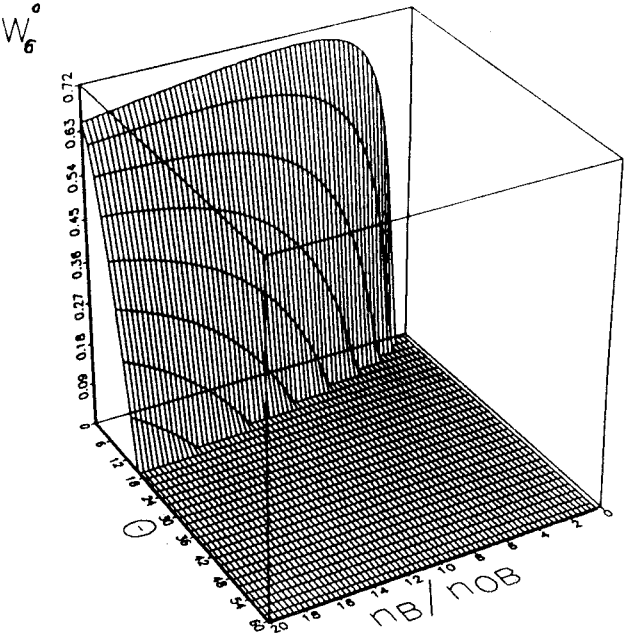

Fig.46. The probability of condensed six-quark clusters

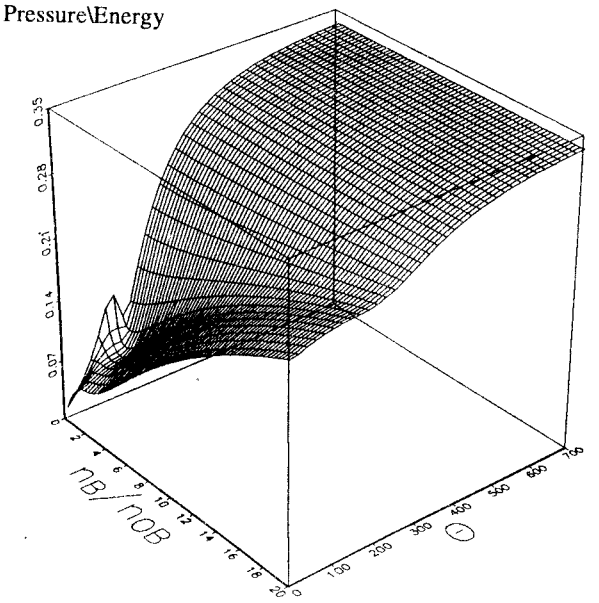

Fig.47. Pressure-to-energy ratio on the temperature-baryon density plane

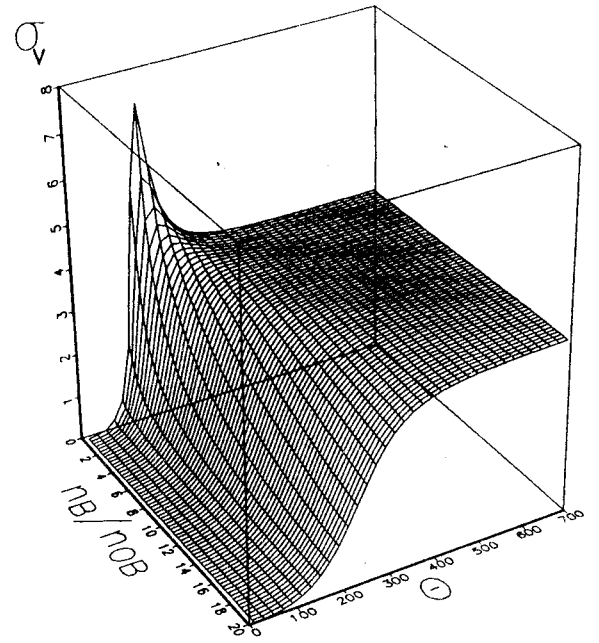

Fig.48. Reduced specific heat

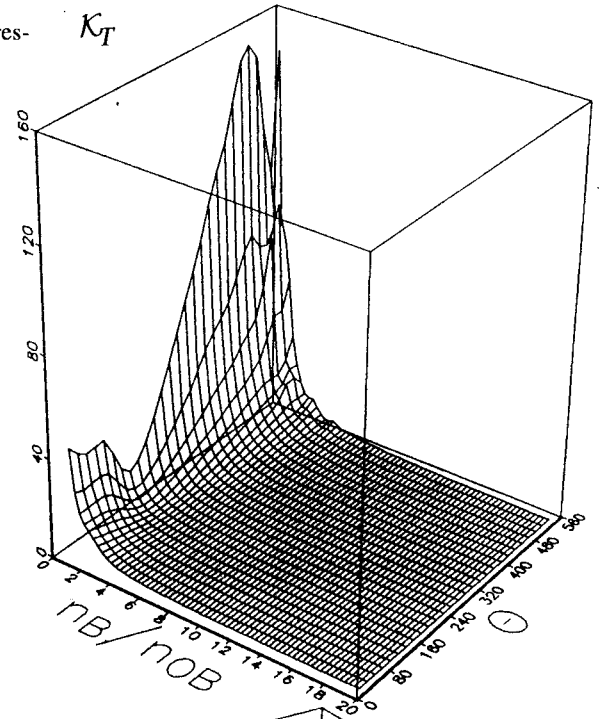

Fig.49. Dimensionless compressibility coefficient

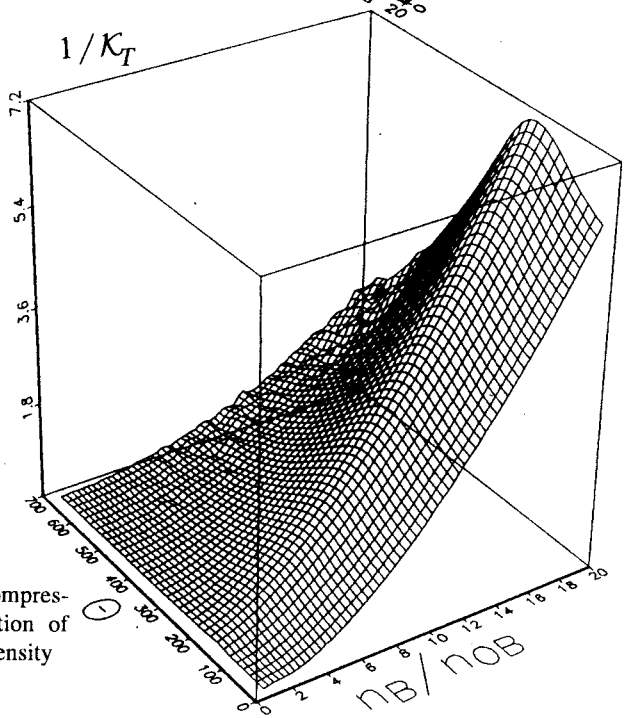

Fig.50. Dimensionless compression modulus as a function of temperature and baryon density

$J = 175\ MeV$ and $\Phi_{22} = 38.42\ GeV/fm^3$, so that $\Phi = 9.61\ GeV/fm^3$. The results of our calculations [148-151] are shown in Figs.35-37 for the quadratic confinement, $\nu \approx 2$. Actually, the results do not change much in the interval $1.5 \leq \nu \leq 2$. We have mainly used $\nu = 1.86$. Deconfinement is a second–order transition at $\Theta_d = 210\ MeV$. As is seen, the agreement with the lattice simulations [135] is beautiful.

15.3. SU(3) Gluon–Glueball Mixture. For the gluon degeneracy factor we have $\zeta_g = 16$. The power ν of the confining interaction is, as in the previous subsection, close to quadratic. But the fitting parameters are $J = 225\ MeV$ and $\Phi = 3.84\ GeV/fm^3$. The glueball characteristics are again taken from Table 2. Calculations show [148,149] that a first–order transition occurs at $\Theta_d = 225\ MeV$ with the relative latent heat $\Delta\varepsilon_d/\varepsilon_{SB} = 0.23$. The agreement with the Monte Carlo lattice simulations [50,51,152] is also very good (Figs.38,39).

15.4. Mixed Quark–Gluon–Meson System. Consider the case of zero baryon density, $n_B = 0$. Take the quarks of two flavours, u and d, and the related antiquarks, $\bar{u}$ and $\bar{d}$. Assume, for simplicity, that all their masses are equal, $m_u = m_d = 7\ MeV$. The degeneracy factor for each kind of quarks is $\zeta_u = \zeta_d = 2N_c = 6$. This factor for gluons is $\zeta_g = 16$. Hadrons are represented by mesons from Tables 3 and 4. Following Section 11, we accept $\Phi_{33} = 315\ MeV/fm^3$, so that $\Phi = \Phi_{33}/9 = 35\ MeV/fm^3$. The plasma interaction parameter $J = 225\ MeV$ is the same as in the previous subsection, as well as $\nu \approx 2$ corresponding to quadratic confinement. So, here we do not add any new fitting parameters.

Our calculations [148,149] displayed in Fig.40 prove that there is no sharp phase transition but there is a gradual crossover. The deconfinement transition can be attributed to the temperature $\Theta_d = 150\ MeV$ where the relative specific heat C_V/C_{SB} has a maximum. The latter is finite and look rather as a Schottky anomaly [153] than as a narrow divergent peak typical of a second–order phase transition. The agreement of our results with the lattice–simulation data [137] is again quite good. The lattice results [137] indicate that the deconfinement transition is really continuous. From the point of view of QCD this can be understood as follows. The role of the quark term in the QCD Lagrangian is similar to that of an external magnetic field applied to a spin system. In the presence of a magnetic field, the ferromagnet–paramagnet transition in simple spin systems becomes a continuous crossover.

15.5. Finite Baryon Density. Here we extend the consideration to nonzero baryon density. The parameters J and Φ are the same as in the previous subsection. Again, we study the two–flavour case with the same characteristics. We take mesons from Table 3, protons and neutrons from Table 5, and multi-quarks from Table 1. For a six–quark cluster we accept $m_6 = 1944\ MeV$. The Bose–Einstein condensate of six–quarks occurs when $\omega_6(0) = 0$. Then, the

baryon potential is

$$\mu_B = \frac{1}{2} m_6 + 3\Phi\rho_{cl} + 3J^{1+\nu}\left(\rho^{-\nu/3} + \rho_{cl}^{-\nu/3}\right),$$

and the density of six–quarks consists of two terms:

$$\rho_6 = \frac{\zeta_6}{(2\pi)^3}\int n_6(k) d\vec{k} + \rho_6^0 .$$

We have analysed the behaviour of several probabilities [154-157] as functions of temperature Θ and relative baryon density n_B/n_{0B}. This is demonstrated in Fig.41 for the plasma probability

$$w_{pl} = \frac{1}{\rho}\left(\rho_g + \rho_u + \rho_{\bar{u}} + \rho_d + \rho_{\bar{d}}\right),$$

in Fig.42 for the pion probability

$$w_\pi = \frac{2}{\rho}\left(\rho_{\pi^+} + \rho_{\pi^-} + \rho_{\pi^0}\right),$$

in Fig.43 for a summarized, excluding pions, probability of other mesons

$$w_{\eta\rho\omega} = \frac{2}{\rho}\left(\rho_\eta + \rho_{\rho^+} + \rho_{\rho^-} + \rho_{\rho^0} + \rho_\omega\right) \equiv w_{mes},$$

in Fig.44 for the nucleon probability

$$w_3 = \frac{3}{\rho}\left(\rho_p + \rho_{\bar{p}} + \rho_n + \rho_{\bar{n}}\right),$$

in Fig.45 for the six–quark probability

$$w_6 = \frac{6}{\rho}\left(\rho_6 + \rho_{\bar{6}}\right),$$

and in Fig. 46 for the probability of condensed six–quark clusters

$$w_6^0 = \frac{6}{\rho}\rho_6^0 .$$

In addition, we present here some other thermodynamic characteristics permitting to better understand the features of the deconfinement transition. The ratio of pressure over energy density, which has the meaning of the effective sound velocity squared,

$$c_{eff}^2 = \frac{p}{\varepsilon},$$

is given in Fig. 47. At $n_B = 0$ the temperature dependence of c_{ef}^2 agrees with that reconstructed from the lattice data [158]. The reduced specific heat

$$\sigma_V = \frac{\Theta}{\varepsilon}\frac{\partial \varepsilon}{\partial \Theta}$$

and the dimensionless compressibility coefficient

$$\kappa_T = \left(\frac{n_B}{J^4}\frac{\partial p}{\partial n_B} \right)^{-1}$$

are depicted in Figs. 48 and 49, respectively. The transition line can be ascribed to the maximum of the inverse compressibility coefficient κ_T^{-1} which can be called [111] the compression modulus (see Fig.50).

We shall not discuss in detail the peculiarities of the calculated thermodynamic functions. This is because, as we think, the presented figures already give a good visual demonstration, and also in order not to make this review too long. Let us only emphasize that the deconfinement transition is a continuous crossover becoming smoother and smoother with increasing baryon density. The deconfinement at a fixed low temperature and rising baryon density is due to the disintegration of hadrons into unbound quarks. When both temperature and baryon density increase, the deconfinement is a result of the hadron disintegration as well as of the generation from vacuum of quarks and gluons.

Concluding we may state that taking into account the coexistence of hadrons and of the quark–gluon plasma is vitally important for constructing a unified approach being in agreement with the lattice–simulation data. The gradual character of the deconfinement transition, occurring through a mixed hadron–plasma state, rules out those predictions that have been based on a sharp first–order phase transition. This concerns the interpretation of signals of the quark–gluon plasma at heavy ion collisions [8-14,159] and the hadronization scenario related to the evolution of early universe after the Big Bang [4]. The quantitative predictions of our approach can be improved in several ways, for instance, by including more kinds of particles or by invoking more elaborate interaction potentials [160]. However, we do hope that qualitatively the picture will remain the same.

Acknowledgements

We are greatly indebted to A.M.Baldin for sparking one of the authors (V.I.Y.) by the problem considered, permanent support and many valuable advices. We acknowledge, with pleasure and gratitude, a number of fruitful discussions with our colleagues from the Relativistic Nuclear Physics Group at Dubna, especially to V.V.Burov, V.K.Lukyanov, and A.I.Titov. We appreciate the help of our coauthors collaborating with us at different stages of our work.

REFERENCES

1. **Baldin A.M.** – Phys. Part. Nucl., 1977, vol.8, p.429.
2. **Shuryak E.V.** – Phys. Rep., 1980, vol.61, p.71.
3. **Gross D.J., Pisarski R.D., Yaffe L.G.** – Rev. Mod. Phys., 1981, vol.53, p.43.
4. **Cleymans J., Gavai R., Suhonen E.** – Phys. Rep., 1986, vol.130, p.217.
5. **McLerran L.** – Rev. Mod. Phys., 1986, vol.58, p.1021.
6. **Müller B.** – Rep. Prog. Phys., 1995, vol.58, p.611.
7. **Reeves H.** – Phys. Rep., 1991, vol.201, p.335.
8. **Halzen F.** – Contemp. Phys., 1983, vol.24, p.591.
9. **Csernai L.P., Kapusta J.I.** – Phys.Rep., 1986, vol.131, p.233.
10. **Stöck R.** – Phys. Rep., 1986, vol.135, p.260.
11. **Stöcker H., Greiner W.** – Phys. Rep., 1986, vol.137, p.277.
12. **Clare R., Strottman D.** – Phys. Rep., 1986, vol.141, p.177.
13. **Koch P., Müller B., Rafelski J.** – Phys. Rep., 1986, vol.142, p.167.
14. **Geiger K.** – Phys. Rep., 1995, vol.258, p.237.
15. **Yukalov V.I.** – Phys. Rep., 1991, vol.208, p.395.
16. **Isaev P.S.** – Quantum Electrodynamics at High Energies, Am. Inst. Phys., New York, 1989.
17. **Sterman G. et. al.** – Rev. Mod. Phys., 1995, vol.67, p.157.
18. **Fermi E.** – Prog. Theor. Phys., 1950, vol.5, p.570.
19. **Hagedorn R.** – Nuovo Cimento Suppl., 1965, vol.3, p.147.
20. **Hagedorn R., Montvay I., Rafelski J.** – Hadronic Matter at Extreme Energy Density, eds. Cabibbo N., Sertorio L., Plenum, New York, 1980, p.49.
21. **Collins J.C., Perry M.J.** – Phys. Rev. Lett., 1975, vol.34, p.1353.
22. **Wong C.W.** – Phys. Rep., 1986, vol.136, p.1.
23. **Baacke J.** – Acta Phys. Pol. B, 1977, vol.8, p.625.
24. **Stauffer D.** – Introduction to Percolation Theory, Taylor and Francis, London, 1985.
25. **Gorenstein M.I., Lipskikh S.A., Zinovjev G.M.** – Z. Phys. C, 1984, vol.18, p.13.
26. **Lieb E.H.** – Bull. Am. Math. Soc., 1990, vol. 22, p.1.
27. **Jackson A., Wetting T.** – Phys. Rep., 1994, vol.237, p.325.
28. **Negele J.W.** – Rev. Mod. Phys., 1982, vol.54, p.913.
29. **Shuryak E.V.** – Phys. Rep., 1984, vol.115, p.151.
30. **Emelyanov V.M., Nikitin Y.P., Vanyashin A.V.** – Fortschr. Phys., 1990, vol.38, p.1.
31. **Källman C.G.** – Phys. Lett. B, 1984, vol. 134, p.363.
32. **Moskalenko I.V., Kharzeev D.E.** – Yad. Fiz., 1988, vol.48, p.1122.
33. **Yukalov V.I.** – Int. J. Mod. Phys. B, 1989, vol.3, p.1691.
34. **Yukalov V.I.** – Physica A, 1990, vol.167, p.833.
35. **Yukalov V.I.** – Phys. Rev. A, 1990, vol.42, p.3324.
36. **Yukalov V.I.** – J. Math. Phys., 1991, vol.32, p.1235.

37. **Yukalov V.I.** – J. Math. Phys., 1992, vol.33, p.3994.
38. **Yukalov V.I., Yukalova E.P.** – Nuovo Cimento B, 1993, vol.108, p.1017.
39. **Yukalov V.I., Yukalova E.P.** – Physica A, 1994, vol.206, p.553.
40. **Yukalov V.I., Yukalova E.P.** – Laser Phys., 1995, vol.5, p.154.
41. **Godwal B., Sikha S., Chidambaram R.** – Phys. Rep., 1983, vol.102, p.121.
42. **Kogut J.B.** – Phys. Rep., 1980, vol.67, p.67.
43. **Engels J ., Karsch F., Satz H., Montvay I.** – Nucl. Phys. B, 1982, vol.205, p.545.
44. **Brown F.R.** – Nucl. Phys. B Proc. Suppl., 1989, vol.9, p.311.
45. **Deng Y.** – Nucl. Phys. B Proc. Suppl., 1989, vol.9, p.334.
46. **Engels J., Fingberg J., Weber M.** – Nucl. Phys. B Proc. Suppl., 1989, vol.9, p.378.
47. **Peterson B.** – Nucl. Phys. A, 1991, vol.525, p.237.
48. **Gottlieb S.** – Nucl. Phys. B Proc. Suppl., 1991, vol. 20, p.247.
49. **Vaccarino A.** – Nucl. Phys. B Proc. Suppl., 1991, vol.20, p.263.
50. **Engels J.** – Nucl. Phys. B Proc. Suppl., 1991, vol.20, p.325.
51. **Karsch F., Laermann E.** – Rep. Prog. Phys., 1993, vol.56, p.1347.
52. **Engels J., Karsch F., Redlich K.** – Nucl. Phys. B, 1995, vol.435, p.295.
53. **Rischke D. H.** – Nucl. Phys. A, 1995, vol.583, p.663.
54. **Yukalov V.I., Shumovsky A.S.** – Lectures on Phase Transitions, World Scientific, Singapore, 1990.
55. **Shuryak E.V.** – Rev. Mod. Phys., 1993, vol.65, p.1.
56. **DeTar C.** – Phys. Rev. D, 1985, vol.32, p.276.
57. **DeGrand T.A., DeTar C.E.** – Phys. Rev. D, 1986, vol.34, p.2469.
58. **DeGrand T.A., DeTar C.E.** – Phys. Rev. D, 1987, vol.35, p.742.
59. **DeTar C.E., Kogut J.B.** – Phys. Rev. D, 1987, vol.36, p.2828.
60. **DeTar C.** – Phys. Rev. D, 1988, vol.37, p.2328.
61. **Hatsuda T., Kunihiro T.** – Phys. Lett. B, 1984, vol.145, p.7.
62. **Hatsuda T., Kunihiro T.** – Phys. Rev. Lett, 1985, vol.55, p.158.
63. **Hatsuda T., Kunihiro T.** – Prog. Theor. Phys., 1985, vol.74, p.765.
64. **Hatsuda T., Kunihiro T.** – Phys. Lett. B, 1987, vol.185, p.304.
65. **Ivlev B.I., Kopnin N.B.** – Usp. Fiz. Nauk, 1984, vol.142, p.435.
66. **Volovik G.E.** – Usp. Fiz. Nauk, 1984, vol.143, p.73.
67. **Schäfer T., Shuryak E.V.** – Phys. Lett. B, 1995, vol.356, p.147.
68. **Adami C., Brown G.E.** – Phys. Rep., 1993, vol.234, p.1.
69. **Kogut J.B., Sinclair D.K., Wang K.C.** – Phys. Lett. B, 1991, vol.263, p.101.
70. **Clark J., Cleymans J., Rafelski J.** – Phys. Rev. C, 1986, vol.33, p.703.
71. **Bi P.Z., Shi Z.P.** – Phys. Rev. C., 1988, vol.38, p.1069.
72. **Kumar A., Krishnamurthy H., Gopal E.** – Phys. Rep., 1983, vol.98, p.58.
73. **De Leeuw F., Van den Doel R., Enz U.** – Rep. Prog. Phys., 1980, vol.43, p.689.

74. **Bunatyan G.G.** – Yad. Fiz., 1986, vol.43, p.294.

75. **Bunatyan G.G.** – Yad. Fiz., 1990, vol.51, p.1243.

76. **Horowitz C.J.** – Phys. Lett. B, 1985, vol.162, p.25.

77. **Oka M., Horowitz C.J.** – Phys. Rev. D, 1985, vol.31, p.2773.

78. **Watson P.J.S.** – Nucl. Phys. A, 1989, vol.494, p.543.

79. **Horowitz C.J., Piekarewicz J.** – Phys. Rev. C, 1991, vol.44, p.2753.

80. **Horowitz C.J., Piekarewicz J.** – Nucl. Phys. A, 1992, vol.536, p.669.

81. **Gardner S., Horowitz C.J., Piekarewicz J.** – Phys. Rev. C, 1994, vol.50, p.1137.

82. **Nzar M., Hoodbhoy P.** – Phys. Rev. C, 1990, vol.42, p.1778.

83. **Melendez W., Horowitz C.J.** – Comp. Phys., 1995, vol.9, p.450.

84. **Enderby J.E., Neilson G.W.** – Adv. Phys., 1980, vol.29, p.323.

85. **Enderby J.E.** – Contemp. Phys., 1983, vol.24, p.561.

86. **Yukalov V.I.** – Theor. Math. Phys., 1973, vol.17, p.1244.

87. **Yukalov V.I.** – Problems in Quantum Field Theory, ed. Bogolubov N.N., Joint Inst. Nucl. Res., Dubna, 1987, p.62.

88. **Yukalov V.I.** – Int. J. Theor. Phys., 1989, vol.28, p.1237.

89. **Yukalov V.I.** – Nuovo Cimento A, 1990, vol.103, p.1577.

90. **Blaschke D., Reinholz F., Röpke G., Kremp D.** – Phys. Lett. B, 1985, vol.151, p.439.

91. **Röpke G., Blaschke D., Schulz H.** – Phys. Rev. D, 1986, vol.34, p.3499.

92. **Röpke G., Blaschke D., Schulz H.** – Phys. Lett. B, 1988, vol.202, p.479.

93. **Röpke G., Blaschke D., Schulz H.** – Phys. Rev. D, 1988, vol.38, p.3589.

94. **Röpke G., Münchow L., Schulz H.** – Nucl. Phys. A, 1982, vol.379, p.536.

95. **Röpke G., Schmidt M., Münchow L., Schulz H.** – Nucl. Phys. A, 1983, vol.399, p.587.

96. **Glyde H.R., Keech G.H.** – Ann. Phys., 1980, vol.127, p.330.

97. **Boyce J.B., Huberman B.A.** – Phys. Rep., 1979, vol.51, p.189.

98. **Chen H.S.** – Rep. Prog. Phys., 1980, vol.43, p.353.

99. **Glendenning N.K.** – Phys. Rev. D, 1992, vol.46, p.1274.

100. **Burov V.V., Lukyanov V.K., Titov A.I.** – Phys. Part. Nucl., 1984, vol.15, p.1249.

101. **Bakker B.L., Narodetskii I.M.** – Adv. Nucl. Phys., 1994, vol.21, p.1.

102. **Baldin A.M., Nazmitdinov R.G., Chizhov A.V., Shumovsky A.S., Yukalov V.I.** – Phys. Dokl., 1984, vol.29, p.952.

103. **Baldin A.M., Nazmitdinov R.G., Chizhov A.V., Shumovsky A.S., Yukalov V.I.** – Multiquark Interactions and Quantum Chromodynamics, ed. Baldin A.M., Joint Inst. Nucl. Res., Dubna, 1984, p.531.

104. **Chizhov A.V., Nazmitdinov R.G., Shumovsky A.S., Yukalov V.I.** – JINR Rapid Commun., 1985, N7, p.45.

105. **Baldin A.M., Shumovsky A.S., Yukalov V.I.** – Phys. Many–Part. Syst., 1986, vol.10, p.10.

106. **Chizhov A.V., Nazmitdinov R.G., Shumovsky A.S., Yukalov V.I.** – Nucl.Phys.A, 1986, vol.449, p.660.

107. **Troian Y.A., Nikitin A.V., Pechenov V.N., Beznogikh Y.D., Doroshenko A.G., Tsarenkov A.P.** – Yad. Fiz., 1991, vol.54, p.1301.

108. **Jaffe R.L.** – Phys. Rev. Lett., 1977, vol.38, p.195.

109. **Matveev V.A., Sorba P.** – Nuovo Cimento A, 1978, vol.45, p.257.

110. **Shanenko A.A., Shumovsky A.S., Yukalov V.I.** – Int. J. Mod. Phys. A, 1989, vol.4, p.2235.

111. **Blaizot J.P.** – Phys. Rep., 1980, vol.64, p.171.

112. **Kukulin V.I., Pomerantsev V.N.** – Prog. Theor. Phys., 1992, vol.88, p.159.

113. **Mchleidt R., Holinde K., Elster C.** – Phys. Rep., 1987, vol.149, p.1.

114. **Yukalov V.I.** – Rep. Inst. Sci. Tech. Inf., 1975, N3684, p.1.

115. **Shanenko A.A., Yukalov V.I.** – Relativistic Nuclear Physics and Quantum Chromodynamics, ed. Baldin A.M., Joint Inst. Nucl. Res., Dubna, 1988, vol.1, p.445.

116. **Kadantseva E.P., Shanenko A.A., Yukalov V.I.** – Selected Topics in Statistical Mechanics, ed. Logunov A.A., World Scientific, Singapore, 1990, p.412.

117. **Kadantseva E.P., Shanenko A.A., Yukalov V.I.** – Phys. Lett. B, 1991, vol.255, p.427.

118. **Kadantseva E.P., Shanenko A.A., Yukalov V.I.** – Relativistic Nuclear Physics and Quantum Chromodynamics, eds. Baldin A.M., Burov V.V., Kaptari L.P., World Scientific, Singapore, 1991, p.602.

119. **Yukalov V.I., Kadantseva E.P., Shanenko A.A.** – Nuovo Cimento A, 1992, vol.105, p.371.

120. **Vary J.P.** – Nucl. Phys. A, 1984, vol.418, p.195.

121. **Bernard C. et al.** – Phys. Rev. Lett., 1992, vol.68, p.2125.

122. **Yukalov V.I., Yukalova E.P., Shanenko A.A.** – Symmetry Methods in Physics, eds. Sissakian A.N., Pogosyan G.S., Vinitsky S.I., Joint Inst. Nucl. Res., Dubna, 1994, vol.2, p.592.

123. **Kadantseva E.P., Shanenko A.A., Yukalov V.I.** – Standard Model and Beyond, eds. Dubnicka S., Ebert D., Sazonov A., World Scientific, Singapore, 1991, p.201.

124. **Kadantseva E.P., Shanenko A.A., Yukalov V.I.** – Phys. At. Nucl., 1992, vol.55, p.435.

125. **Shanenko A.A., Yukalova E.P., Yukalov V.I.** – Hadronic J., 1993, vol.16, p.1.

126. **Au K.L., Morgan D., Pennington M.R.** – Phys. Lett. B, 1986, vol.167, p.229.

127. **Boutemer M., Peigneux J.** – Nucl. Phys. B Proc. Suppl., 1991, vol.21, p.159.

128. **Kogut J., Sinclair D., Susskind L.** – Nucl. Phys. B, 1976, vol.114, p.199.

129. **Berg B., Billoire A.** – Nucl. Phys. B, 1983, vol.221, p.109.

130. **Gupta R., Patel A., Baillie C., Kilcup G., Sharpe S.** – Phys. Rev. D, 1991, vol.43, p.2301.

131. **Fritzsch H., Minkowski P.** – Nuovo Cimento A, 1975, vol.30, p.393.

132. **Jaffe R., Johnson K.** – Phys. Lett. B, 1975, vol.60, p.201.

133. **Donoghue J., Johnson K., Li B.** – Phys. Lett. B, 1981, vol.99, p.416.

134. **Engels J., Karsch F., Montvay I., Satz H.** – Phys. Lett. B, 1981, vol. 101, p.89.

135. **Engels J., Finberg J., Redlich K., Satz H., Weber M.** – Z. Phys. C, 1989, vol.42, p.341.

136. **Brown F., Christ N., Deng Y., Gao M., Woch T.** – Phys. Rev. Lett., 1988, vol.61, p.2058.

137. **Çelik T., Engels J., Satz H.** – Nucl. Phys. B, 1985, vol.256, p.670.

138. **Ter Haar D.** – Elements of Statistical Mechanics, Rinehart, New York, 1954.

139. **Zimányi J., Lukács B., Lévai P., Bondorf J., Balazs N.** – Nucl. Phys. A, 1988, vol.484, p.647.

140. **Rischke D.H., Friman B.L., Stöcker H., Greiner W.** – J.Phys. G, 1988, vol.14, p.191.

141. **Shanenko A.A., Yukalova E.P., Yukalov V.I.** – Physica A, 1993, vol.197, p.629.

142. **Shanenko A.A., Yukalova E.P., Yukalov V.I.** – Symmetry and Structural Properties of Condensed Matter, eds. Florek W., Lipinski D., Lulek T., World Scientific, Singapore, 1993, p.237.

143. **Eichten E., Gottfried K., Kinoshita T., Lane K., Yan T.** – Phys. Rev. D, 1978, vol.17, p.3090.

144. **Eichten E., Gottfried K., Kinoshita T., Lane K., Yan T.** – Phys. Rev. D, 1980, vol.21, p.203.

145. **Simonov Y.A.** – Yad. Fiz., 1991, vol.54, p.192.

146. **Ding H.Q.** – Int. J. Mod. Phys. C, 1991, vol.2, p.637.

147. **Mukherjee S., Nag R., Sanyal S., Morii T., Morishita J., Tsuge M.** – Phys. Rep., 1993, vol.231, p.201.

148. **Shanenko A.A., Yukalova E.P., Yukalov V.I.** – Phys. At. Nucl., 1993, vol.56, p.372.

149. **Shanenko A.A., Yukalova E.P., Yukalov V.I.** – Nuovo, Cimento A, 1993, vol.106, p.1269.

150. **Shanenko A.A., Yukalova E.P., Yukalov V.I.** – Proceedings of Workshop on Soft Physics, eds. Bugrij G., Jenkovsky L., Martynov E., Ukr. Acad. Sci., Kiev, 1993, p.111.

151. **Shanenko A.A., Yukalova E.P., Yukalov V.I.** – Relativistic Nuclear Physics and Quantum Chromodynamics, eds. Baldin A.M., Burov V.V., Joint Inst. Nucl. Res., Dubna, 1994, p.191.

152. **Brown F.R. et al.** – Phys. Rev. Lett., 1990, vol.65, p.2491.

153. **Barron T.H., Collins J.G., White G.K.** – Adv. Phys., 1980, vol.29, p.609.

154. **Shanenko A.A., Yukalova E.P., Yukalov V.I.** – Hadrons and Nuclei from Quantum Chromodynamics, eds. Fujii K., Akaishi Y., Reznik B., World Scientific, Singapore, 1994, p.109.

155. **Shanenko A.A., Yukalova E.P., Yukalov V.I.** – Phys. Dokl., 1995, vol.40, p.291.

156. **Shanenko A.A., Yukalova E.P., Yukalov V.I.** – Phys. At. Nucl., 1995, vol.58, p.335.

157. **Shanenko A.A., Yukalova E.P., Yukalov V.I.** – JINR Rapid Commun., 1995, N69, p.19.

158. **Mornas L., Ornik U.** – Nucl. Phys. A, 1995, vol.587, p.828.

159. **Singh C.P.** – Phys. Rep., 1993, vol.236, p.147.

160. **Hjorth–Jensen M., Kuo T., Osnes E.** – Phys. Rep., 1995, vol.261, p.125.